Tunning processes for organic matter removal from slaughterhouse wastewater treated by immediate one-step lime precipitation and atmospheric carbonation

Luís Madeira [a,b,c], Adelaide Almeida [b,d], Ana Maria Rosa da Costa [a,e], Ana S. Mestre [f], Fátima Carvalho [b,d], Margarida Ribau Teixeira [a,c,*]

[a] *Faculdade de Ciências e Tecnologia, Universidade do Algarve, Edifício 7, Campus de Gambelas, 8005-139 Faro, Portugal*
[b] *Departamento de Tecnologias e Ciências Aplicadas, IPBeja, Ap. 158, 7801-902 Beja, Portugal*
[c] *CENSE, Center for Environmental and Sustainability Research, Portugal & CHANGE, Global Change and Sustainability Institute, Portugal*
[d] *FiberEnTech, Fiber Materials and Environmental Technologies, Universidade de Beira Interior, Covilhã, Portugal*
[e] *CEOT – Centre for Electronics, Optoelectronics and Telecommunications, Campus de Gambelas, 8005-139 Faro, Portugal*
[f] *Centro de Química Estrutural, Institute of Molecular Sciences, Departamento de Química e Bioquímica, Faculdade de Ciências, Universidade de Lisboa, Campo Grande, Lisboa 1749-016, Portugal*

ARTICLE INFO

ABSTRACT

Adsorption using unmodified/modified commercial activated carbons and constructed wetlands (CW) planted with *Vetiveria zizanioides* were evaluated as tuning processes for lowering chemical oxygen demand (COD) from slaughterhouse wastewater pretreated by the integrated process of immediate one-step lime precipitation and atmospheric carbonation. Powdered and granular activated carbons (PAC and GAC), and PAC and GAC incorporated with iron oxide nanoparticles (PACMAG and GACMAG) were used. COD removal using different adsorbent separation methods (i.e., sedimentation, filtration, or magnetic separation) was also evaluated. The adsorption results indicated that the best adsorbent doses and contact times of the studied adsorbents were 70 g L^{-1} and 5 min for PAC and PACMAG, and 60 g L^{-1} and 60 min for GAC and GACMAG. Under optimized conditions, GAC (75.7 $\pm$ 1.0%) and GACMAG (73.5 $\pm$ 2.1%) were more efficient than PAC (59.7 $\pm$ 1.0%) and PACMAG (59.0 $\pm$ 0.0%) in removing COD. The incorporation of iron oxide nanoparticles in GAC and PAC did not affect the adsorption of COD. The Temkin model was the best isotherm model found for PAC and PACMAG, while for GAC and GACMAG was the BET model. Pseudo-order n kinetic model was the best kinetic model found for all the adsorbents tested. There were no significant differences in the removal of COD between filtration and magnetic separations. Phytoremediation results indicated that increased COD removal efficiency occurred when the applied COD mass load decreased or when the bed depth was increased. Maximum COD removals of around 89.9–95.0% were achieved. *Vetiveria zizanioides* showed no signs of toxicity throughout the trials.

1. Introduction

Slaughterhouse wastewater (SWW) is a complex effluent characterized by a high content of organic matter, nutrients (nitrogen and phosphorus), oils and fats, total suspended solids (TSS), and microorganisms [1]. Therefore, it is a challenge to find efficient, economic, low-energy, ecological, and simple treatment processes. Different SWW treatment processes have been investigated, namely: i) physical-chemical treatments (e.g., coagulation and flocculation, dissolved air flotation, electrocoagulation, adsorption, membranes, and acid precipitation [2]); ii)

biological treatments (e.g., activated sludge (AS), anaerobic filters and constructed wetlands (CW)); iii) chemical oxidation processes (e.g., ozonation); iv) advanced oxidation processes (AOP) (e.g., UV-H_2O_2, gamma radiation, Fenton, photo-Fenton and electro-Fenton); and v) combined processes (e.g., coagulation/adsorption, AS/reverse osmosis, anaerobic baffled reactor (ABR)/UV/H_2O_2, ABR/aerobic AS/UV/H_2O_2, anaerobic lagoon/CW, anaerobic digestion/CW and coagulation/electro-Fenton [3]). Combined processes have shown better performance than individual treatments since the last ones complement each other to remove contaminants [4]. Recently, Madeira et al.

[5] developed a low-cost and easy-to-apply pretreatment for SWW, using a combined immediate one-step lime precipitation (IOSLM) and atmospheric carbonation (AC) process. These authors obtained removals higher than 80% for chemical oxygen demand (COD) and biochemical oxygen demand (BOD). To fulfill discharge requirements, this combined process needs to be complemented with a refining process. Reverse osmosis and AOP are highly effective in removing organic matter, but they have high capital and operating/maintenance costs [6,7]. Biological treatments are low-cost and simple, but they are not suitable for removing some poorly biodegradable contaminants [1,8]. So, adsorption and phytoremediation are treatment processes that could be a solution, however, their effectiveness for safe discharge into water bodies is still questioned [9].

Adsorption is a low-cost, high-performance, and easy operational design process that has been used to remove a wide range of organic (e.g., dyes, pesticides, herbicides, drugs, and other emerging contaminants) and inorganic (e.g., heavy metals, radionuclides, etc.) [10]. Different adsorbents have been used in adsorption, like activated carbons (powdered activated carbon (PAC) and granular activated carbon (GAC)), improved biochars, nano adsorbents, metal oxide adsorbents, magnetic adsorbents, hybrid adsorbents, and others [11]. Some COD and BOD removal studies from SWW by adsorption processes using activated carbon and improved biochars have been reported. [12] achieved high COD (92–95%) and BOD (68–69%) removal efficiencies from a poorly biodegradable SWW, using rubber seed pericarp activated carbon and commercially supplied activated carbon. Djonga et al. [13] obtained organic matter removals of 40.7% from SWW when they applied an adsorbent based on Ayous sawdust. About 64% of COD was removed from SWW by Real-Olvera et al. [14] using 7 g L^{-1} of powdered *Moringa oleifera* seeds. Affam et al. [15] observed that greater COD removals from SWW were obtained with iron oxide-coated GAC (ca. 70.7%) than with GAC alone (ca. 27.6%) at 3.5 g L^{-1} of adsorbent and pH 3–7. The modification of activated carbon by iron oxide or iron oxide nanoparticles (NPs) has also been recently investigated to remove organic matter. However, no studies on the application of iron oxide NPs incorporated in activated carbon (PAC or GAC) to remove COD from SWW were found in the literature. Lompe et al. [16] found that the adsorption capacity of iron oxide/activated carbon nanoparticle composite to remove dissolved organic carbon (DOC) from a synthetic solution is reduced proportionally to the mass fraction of PAC in the composite due to the relatively low adsorption capacity of iron oxide NPs for DOC compared to PAC. In fact, unlike mesopores volume (which increased), a decrease in surface area and micropores volume was observed with increasing iron oxide NPs mass fraction incorporated in PAC [16]. Thus, these authors recommend the use of highly mesoporous PAC and small fractions of iron oxide NPs during the synthesis of iron oxide/activated carbon nanoparticle composite. Anyway, the incorporation of iron oxide NPs in PAC is still not very clear, as positive effects on the adsorption capacity of natural organic matter have been found in the literature [17]. The advantage of using iron oxide or iron oxide nanoparticles incorporated in activated carbon is the easy separation of the adsorbent from water using a magnetic field since this composite presents magnetic characteristics, simplicity, high efficiency, and low costs compared to the filtration process [18]. Moreover, some conventional processes of adsorbent separation such as centrifugation, precipitation, filtration, and chromatography are not very economical and require labor [19].

Phytoremediation in constructed wetlands (CW) has also been applied to the SWW [9,20] and pretreated SWW (e.g., from anaerobic-aerobic SBRs [21], septic tank [22] and biodigester [23]). High COD (61.3–97.4%) and BOD (52.4–99.9%) removals from raw-/pretreated SWW using different plant species (such as *Phragmites australis* [20], *Typha latifólia* [9,22], *Cyperus papyrus*, *Miscanthidium violaceum*, *Phragmites mauritianus* and *Typha domingensis* [21]) has been obtained. The plant *Vetiveria zizanioides* has also been highlighted in the phytoremediation of synthetic and real effluents [24] due to its strong resistance and survival to extreme climatic and edaphic conditions (e.g., pH 3–10.5, salinity until 47.5 dS m^{-1}, temperatures ranging from $-9°$ to 55°C, and others) [25-27,24,28]. However, there are few reported cases of its use in the treatment of SWW. Manh et al. (2014) obtained COD and BOD removals of 60% and 59.8%, respectively, using CW planted with *Vetiveria zizanioides* to treat the biodegradable pretreated SWW from a biodigester. However, no information on the effect of some operative variables (e.g., bed depth and applied mass load), on the tuning of poorly biodegradable and alkaline pretreated SWW by CW planted with *Vetiveria zizanioides*, has been found in the literature. Although some authors, such as [29] and [30] have shown that it is possible to use CW planted with *Vetiveria zizanioides* to treat poorly biodegradable and alkaline pretreated wastewaters (e.g., explosives wastewater and landfill leachate) from IOSLM and AC integrated process, the effect of the variables mentioned has not been studied. Since the plant *Vetiveria zizanioides* tolerates wide pH ranges (3–10.5) [25], the application of alkaline effluents in CW could also be an advantage in reducing the carbonation time. Almeida et al. [31] observed that the bed depth and applied mass load can influence the nitrogen removal from synthetic wastewater (at pH 7.5 $\pm$ 0.2) in constructed wetlands planted with *Vetiveria zizanioides*. More information on organic matter removal under these conditions is needed.

This work aims to evaluate the tuning of poorly biodegradable and alkaline pretreated SWW from the IOSLM and AC integrated process for wastewater discharge or reuse, using two processes namely adsorption and phytoremediation.

2. Materials and methods

2.1. Slaughterhouse wastewater sampling

Raw SWW was collected at the output of the rotary drum screen filter in a slaughterhouse located in Portugal. The samples were immediately transferred to the laboratory and were then pretreated by the IOSLM process at pH 12 followed by the AC process, according to [5]. Then, the SWW pretreated by the IOSLM+AC process was used in adsorption tests and phytoremediation tests. If not immediately analyzed, the pretreated samples were stored at 4°C until use. Parameters such as pH, conductivity, COD, soluble chemical oxygen demand (SCOD), BOD, total suspended solids (TSS), ammoniacal nitrogen, and turbidity were determined (see Section 2.4). Table S1 shows the SWW characteristics pretreated by IOSLM+AC processes for the adsorption and phytoremediation tests.

2.2. Magnetite nanoparticles and adsorbent preparation

Magnetite NPs were obtained as described by Vargues et al. (2021). In general, ferric chloride hexahydrate was first dissolved in HCl (2 M) and then mixed with the sodium sulfite solution, under stirring for 30 min, until the initial color of the ferric chloride solution was reached. Then, the above mixture was added to the ammonia solution and kept under strong stirring for 30 min, occurring an immediate precipitation of a black solid. Subsequently, the supernatant was decanted by applying a neodymium magnet to the black precipitate, which was washed once with HCl (0.1 M) and then several times with deionized water until reaching neutral pH. The precipitate was air-dried for 2 days and then macerated for incorporation in activated carbon.

Two commercial activated carbons, one in powdered form (SORBOPOR® MV 118/P and hereinafter referred to as PAC), and another in granular form (NORIT® GAC 830 and hereinafter referred to as GAC), were previously washed with deionized water to remove some soluble impurities. After washing, they were air-dried for 2 days and then stored in a desiccator until use.

Magnetite NPs were incorporated into PAC according to Vargues et al. (2021). For this, the magnetite NPs were sonicated in deionized water for 15 min. Then, the PAC was added to the sonicated NPs (in a

proportion of 0.150 g of magnetite NPs per 0.500 g PAC), under agitation at 1200 rpm. After 15 min, the agitation was interrupted and the sedimentation was started for 10 min, under the action of the neodymium magnet (40×15×5 mm). Subsequently, the PAC with the magnetite NPs (called PACMAG) was washed 10 times with deionized water under the action of a neodymium magnet. Finally, the PACMAG was air-dried for 2 days and then stored in a desiccator until use. The incorporation of magnetite NPs into GAC followed the same procedure was like used for PAC, resulting in GACMAG. Before the adsorption tests, the magnetic properties of PACMAG and GACMAG were certified using a magnet.

2.3. Experimental set-up

An experimental setup for the adsorption process and phytoremediation process is shown in Fig. S1.

2.4. Adsorption tests

Three laboratory-scale batch adsorption assays were made (Table S2, Fig. S1a). The type of adsorbent, dosage, time, and separation method were tested (Table S2). In general, in the adsorption assays, about 5 mL of pretreated SWW by IOSLM+AC process (Table S1) were placed in a sample vial with a predetermined dose of the adsorbent (PAC, PACMAG, GAC, or GACMAG), and then the mixture was shaken in an orbital shaker (Edmund Bühler KS-15) at 250 rpm and room temperature. After the defined contact time, the adsorbents were separated from the effluent using one of the separation methods (Table S2). In the first and second experiments (trials A and B, Table S2) adsorption equilibrium isotherms (dosage at 10–100 g L^{-1}) and adsorption kinetics (0–60 min for PAC and PACMAG and 0–300 min for GAC and GACMAG) were made. Then, the samples were filtered by dead-end microfiltration (using Whatman™ membrane filters with a 0.45 μm pore size) and analyzed for COD. Finally, in the third experiment (trial C, Table S2), the adsorbents (PAC, GAC, PACMAG, and GACMAG) were applied to treat 5 mL of pretreated SWW, in an orbital shaker, using the best adsorption operating conditions (dose and contact time) from first and second experiments. After adsorption, different effluent separation methods were individually applied, namely: gravitational sedimentation, magnetic separation, and dead-end microfiltration. In magnetic separation, a NdFeB block magnet (40 ×15×5 mm) Ni-Cu-Ni coated, with a remanence of 1250–1280 mT and a coercivity of 907 kA/m was used (Supermagnete, Germany). For the separation of PACMAG and GAC-MAC from the supernatant, the magnetic field was applied at the bottom of the sample vial. During the sedimentation and magnetic step, the effluent samples were collected over time and analyzed for COD and turbidity.

2.5. Phytoremediation tests

Two pilot-scale CWs planted with *Vetiveria zizanioides* (>120 plants m^{-2}) in light-expanded clay aggregates (Leca®NR 10/20) were used in the phytoremediation tests (Fig. S1b). Both beds had a surface area of 0.24 m^2 (0.40 ×0.60 m) but different bed heights, 0.35 m for CW1 and 0.70 m for CW2. The effect of bed height and COD and ammonium nitrogen (NH$_4^+$) applied mass load on COD and NH$_4^+$ removal efficiency was evaluated. The tests took place between February and April, and according to the operating conditions applied to the beds shown in Table 1. Both beds were fed in vertical flow, continuous mode, and constant applied hydraulic load around 80 L m^{-2} d^{-1}, using submersible pumps and a network of equidistant sprinklers. Hydraulic retention times were 3.6 ± 0.5 and 7.1 ± 0.9 h, for CW 1 and CW 2, respectively. Air and soil temperatures varied on average from 16 to 23ºC and from 13 to 18ºC, respectively (Table 1). To achieve COD mass loads of 3.2–9.5 g m^{-2} d^{-1} (trials A and B, Table 1), the pretreated SWW by IOSLM+AC process (Table S1) was diluted with tap water and only then fed to both beds. To evaluate the high COD loadings and the importance of SWW pretreatment by the IOSLM+AC process, both CWs were fed with raw SWW (pH 7.85 ± 0.45, conductivity 3.1 ± 0.3 mS cm^{-1}, COD 2648 ± 329 mg O$_2$ L^{-1}, and NH$_4^+$ 48 ± 7 mg N-NH$_4^+$ L^{-1}, see Table 1, trials C). Daily, at 10:00 am, wastewater samples were collected at the inlet and outlet of the bed, and the flow rates were measured. The samples were immediately characterized in terms of pH, redox potential, electrical conductivity, and dissolved oxygen (DO). For NH$_4^+$ and COD, when it was not possible to measure immediately, the samples were refrigerated at 4ºC until further analysis. Signs of *Vetiveria zizanioides* toxicity were evaluated weekly by visual inspection. Plant growth and biomass composition (for calcium, magnesium, sodium, potassium, total Kjeldahl nitrogen, and phosphorus) were evaluated at the beginning and end of the phytoremediation test. For this, twenty plants were randomly selected from each CW. In periods of rain, the beds were covered with thin transparent plastic.

2.6. Analytical methods

The wastewater samples were analyzed according to the standard methods of analysis [32]. pH was measured by the potentiometric method using a WTW pocket pH meter kit (model pH 340). Conductivity was determined by the electrometric method using a Crison GLP32 conductimeter. COD and soluble COD (SCOD) were determined by closed reflux colorimetric method using MACHEREY-NAGEL Thermoblock NANOCOLOR VARIO C2, Thermo scientific Genesys 10 S UV–VIS spectrophotometer, and Whatman™ membrane filter with a 0.45 μm pore size for soluble COD. BOD$_5$ was determined by the respirometric method using the WTP OxiTop® IS 12 system. NH$_4^+$ was obtained by distillation method using BUCHI B-316 distillation unit. TSS were quantified by the gravimetric method using glass microfiber filters (VWR) with a pore size of 1.0 μm and a diameter of 47 mm. Turbidity was determined by the nephelometric method or estimated by absorption of light at 750 nm. Redox potential was measured by the potentiometric method using a WTW Inolab apparatus and WTW SenTix ORP electrode. Dissolved oxygen was quantified by modifications of the Winkler method.

The physicochemical characteristics of the *Vetiveria zizanioides* leaves

Table 1
Operating conditions applied to CW 1 and CW 2.

Type of CW	Trials	Parameters						
		pH	COD (g m^{-2} d^{-1})	NH$_4^+$-N load (g m^{-2} d^{-1})	Hydraulic load (L m^{-2} d^{-1})	HRT (h)	Air temp. (ºC)	Soil temp. (ºC)
CW1	A1	9.48 ± 0.77	4.1 ± 0.5	0.3 ± 0.1			16 ± 1	13 ± 1
	B1	10.25 ± 1.03	9.5 ± 2.2	0.5 ± 0.05	81 ± 10	3.6 ± 0.5	21 ± 3	16 ± 3
	C1	7.85 ± 0.45	211.8 ± 26.4	3.9 ± 0.5			23 ± 5	18 ± 2
CW2	A2	9.48 ± 0.77	3.2 ± 1.1	0.3 ± 0.1			16 ± 1	13 ± 1
	B2	10.25 ± 1.03	9.4 ± 2.5	0.5 ± 0.06	80 ± 10	7.1 ± 0.9	21 ± 3	16 ± 3
	C2	7.85 ± 0.45	211.8 ± 26.4	3.9 ± 0.5			23 ± 5	18 ± 2

Note: Mean ± Standard Deviation, calculated for a 95% confidence level; number of determinations (n ≥ 10).

were quantified according to [33]. First, the leaves were cut into small pieces and placed in an oven (Memmert UL40 Oven) at 70 °C for 48 h for the determination of the dry matter by the gravimetric method. Subsequently, the samples were placed in a muffle furnace at 550 °C for 4 h. The ash obtained was dissolved with hydrochloric acid (3 M), followed by filtration with a Whatman™ 1001 filter, and then diluted with deionized water (for calcium, magnesium, total phosphorus, sodium, and potassium determination). Calcium and magnesium were determined by the flame atomic absorption spectrometry method using Varian SpectrAA 220FS equipment. Sodium and potassium were quantified by the flame photometric method using the Corning Model 410 Flame Photometer. Phosphorus was determined by the colorimetric method using muffle P SELECTA-HORN 186331 and UV/Vis spectrophotometer Pharmacia Biotech Ultrospec 2000. TKN was analyzed by the Kjeldahl method using Bloc Digest 6 P-Selecta digester and BUCHI B-316 distillation unit.

The activated carbon materials were characterized regarding by their morphology, texture, surface chemistry, and physicochemical properties. Morphology was analyzed by scanning electron microscopy (SEM, FEI Quanta 200), using Everhart–Thornley detector. The detection of impurities in activated carbon was evaluated by SEM using a solid-state detector. The presence of iron oxide NPs in PACMAG/GACMAG was assessed by FTIR spectra using Bruker Tensor 27 FT-IR Spectrometer. For this purpose, the adsorbents were mixed with KBr to form pellets, and then the pellets were subjected to transmittance spectra between 4000 and 400 cm^{-1} with baseline correction, resolution of 4 cm^{-1} and 25 scans. The texture was assessed by N$_2$ adsorption at $-$ 196 °C in an Automatic apparatus Micromeritics ASAP 2010. Before data acquisition, $\approx$ 75 mg of the materials were outgassed overnight at 120 °C. The apparent surface area, A_{BET}, was estimated through the Brunauer-Emmett-Teller (BET) method following the recommended practices for microporous solids [34-36]. The total pore volume, V_{total}, was determined through the Gurvich rule at $p/p^0 = 0.975$ [37], and the micropore volume, V_{micro}, was assessed by applying the α_s method taking as reference the isotherm reported by Rodriguez-Reinoso et al. [38], and the mesopore volume, V_{meso}, was obtained from the difference between the total pore volume, V_{total}, and the micropore volume, V_{micro}. The reverse mass titration method [39] was used to determine the pH at the point of zero charge (pH$_{PZC}$). Briefly, the measurements were made with $\approx$ 100 mg of previously dried material with decarbonized deionized water following the methodology described by Mestre et al. [40] and the pH was assessed with a Symphony SP70P pH meter. The moisture content was assessed following the oven drying method (ASTM D2867–04). Each sample was dried at 110 °C in a ventilated oven (Heraeus Instrument) until constant weight. The ash content was determined according to ASTM D2866–99 with correction for the moisture content [41]. Briefly, the samples were heated at 815 °C in air (Select-Horn from Selecta, Omron E5Cx controller), until constant mass. The particle size distribution of the powdered and granular materials was assessed by dry sieving considering the percentage of weight collected in sieves with dimensions between 850 and 20 µm and assuring a total weight loss lower than 10% to guarantee a valid distribution [42, 43]. The apparent density of the powdered activated carbon materials was determined by the tapping method using a graduated cylinder according to the procedure described by Viegas et al. [44]. For granular materials, the sample was added to the graduated cylinder by a vibratory feeder and the cylinder was selected assuring its inner diameter was at least 10 times the mean particle diameter (ASTM2854–2000).

2.7. Statistical analysis

Results were presented as means $\pm$ standard deviation, using n = 3 for the adsorption tests and n $\geq$ 10 for the phytoremediation tests. All samples were analyzed in triplicate. IBM SPSS Statistics for Windows was used for statistical purposes. One-way ANOVA with Tukey's test at a 95% confidence level was used for comparison between averages. Two-

Way ANOVA with Least Significance Difference (LSD) test at a 95% confidence level, was used for the analysis of variance with two factors. Graphs were created using GraphPad Prism for Windows (version 8.0.1, GraphPad Software, Inc.).

In the adsorption tests, different non-linear equations relative to the isotherm adsorption and kinetic adsorption were used to find the best one that portrays the experiments. For that, the sum of squared residuals was minimized using Microsoft Excel Solver and the generalized reduced gradient nonlinear solving method. Langmuir, Freundlich, Redlich-Peterson, Two-site Langmuir, Generalized Freundlich, Langmuir-Freundlich, Toth, Temkin, and BET were the adsorption isotherms used (Table S3). On the other hand, Pseudo-first order, Pseudo-second order, Pseudo-order n (n ǂ 1), Weber and Morris intra-particle diffusion, Elovich, and Bangham were the adsorption kinetics models used (Table S4). For all adsorption isotherms and adsorption kinetics, the average absolute relative deviation percent (AARD) (Eq. (1)), the root-mean-square error (E) (Eq. (2)), and the coefficient of determination (R^2) (Eq. (3)) were calculated. The adsorption capacity of absorbate (q) and the percentage of removal of the absorbate (%R) were determined according to Eqs. (4) and (5), respectively.

$$AARD = \frac{1}{N} \sum_{i=1}^{N} \left(\left| \frac{q_{e.i} - q_{cal.i}}{q_{e.i}} \right| \right) \times 100 \tag{1}$$

$$E = \sqrt{\frac{\sum_{i=1}^{N} (q_{cal.i} - q_{e.i})^2}{N}} \tag{2}$$

$$R^2 = 1 - \frac{\sum_{i=1}^{N} (q_{e.i} - q_{cal.i})^2}{\sum_{i=1}^{N} (q_{e.i} - q_{mean})^2} \tag{3}$$

$$q = \frac{(C_0 - C)}{m} \times V \tag{4}$$

$$\%R = \frac{(C_0 - C)}{C_0} \times 100 \tag{5}$$

where: $q_{e.i}$ and $q_{cal.i}$ are the adsorption capacity of the absorbate obtained by the experimental method and by calculation, respectively; N is the number of experiments; q_{mean} is the average of the $q_{e.}$ values; C_0 and C are the initial and the final concentrations of absorbate (mg L^{-1}), respectively; m is the adsorbent mass (g), and V is the solution volume (L).

In phytoremediation tests, the removal efficiency of each parameter (η) (%) and the hydraulic retention time (HRT) (d) were determined according to Eqs. (6) and (7), respectively.

$$\eta = \frac{(H_{Li} \times C_i - H_{Le} \times C_e)}{H_{Li} \times C_i} \times 100 \tag{6}$$

$$HRT = \frac{V}{Q_i} = \frac{A \times y \times p}{Q_i} \tag{7}$$

where: H_{Li} and H_{Le} are the hydraulic loads at the inlet and outlet of the bed (L m^{-2} d^{-1}), respectively; C_i and C_e are the concentrations of a parameter at the inlet and outlet of the bed (mg L^{-1}), respectively; V is the volume of the bed (m^3); Q_i is the influent flow rate (L d^{-1}); A is the surface area of the bed (m^2); y is the depth of the bed (m); p is the porosity of the bed.

3. Results and discussion

3.1. Characterization of pretreated SWW

The pretreated SWW shows a wide range of pH (7.89–11.10),

conductivity (579–3270 mS cm^{-1}), and ammonium nitrogen (8.4–56.4 mg N L^{-1}) (Table S1). These values are due to sampling at different stages in the atmospheric carbonation process, in which high and low values were associated with the beginning and end of atmospheric carbonation, respectively [5]. The pretreated SWW still has some organic matter (385–507 mg O$_2$ L^{-1} for COD and 80–90 mg O$_2$ L^{-1} for BOD$_5$) that was not removed by the IOSLM+AC process (Table S1). Most of the organic matter is soluble (SCOD at 372–498 mg O$_2$ L^{-1}, Table S1). SWW is a low biodegradable wastewater as it has a BOD$_5$/COD ratio of 0.18–0.21 (Table S1), so it would not be possible to be treated by conventional biological treatment processes. Low biodegradable wastewater from the slaughterhouse has also been found in the literature, with BOD$_5$/COD ratios of 0.30 [15], 0.09, and 0.14 [12], for example. Some SWWs may present low biodegradability due to cleaning activities at the facilities, as mentioned by Ng et al. [45]. In this case, the biodegradability of wastewater was reduced by the IOSLM+AC process [5,46]. Low values of TSS (4–8 mg L^{-1}) and turbidity (0.8–0.9 NTU) were observed (Table S1).
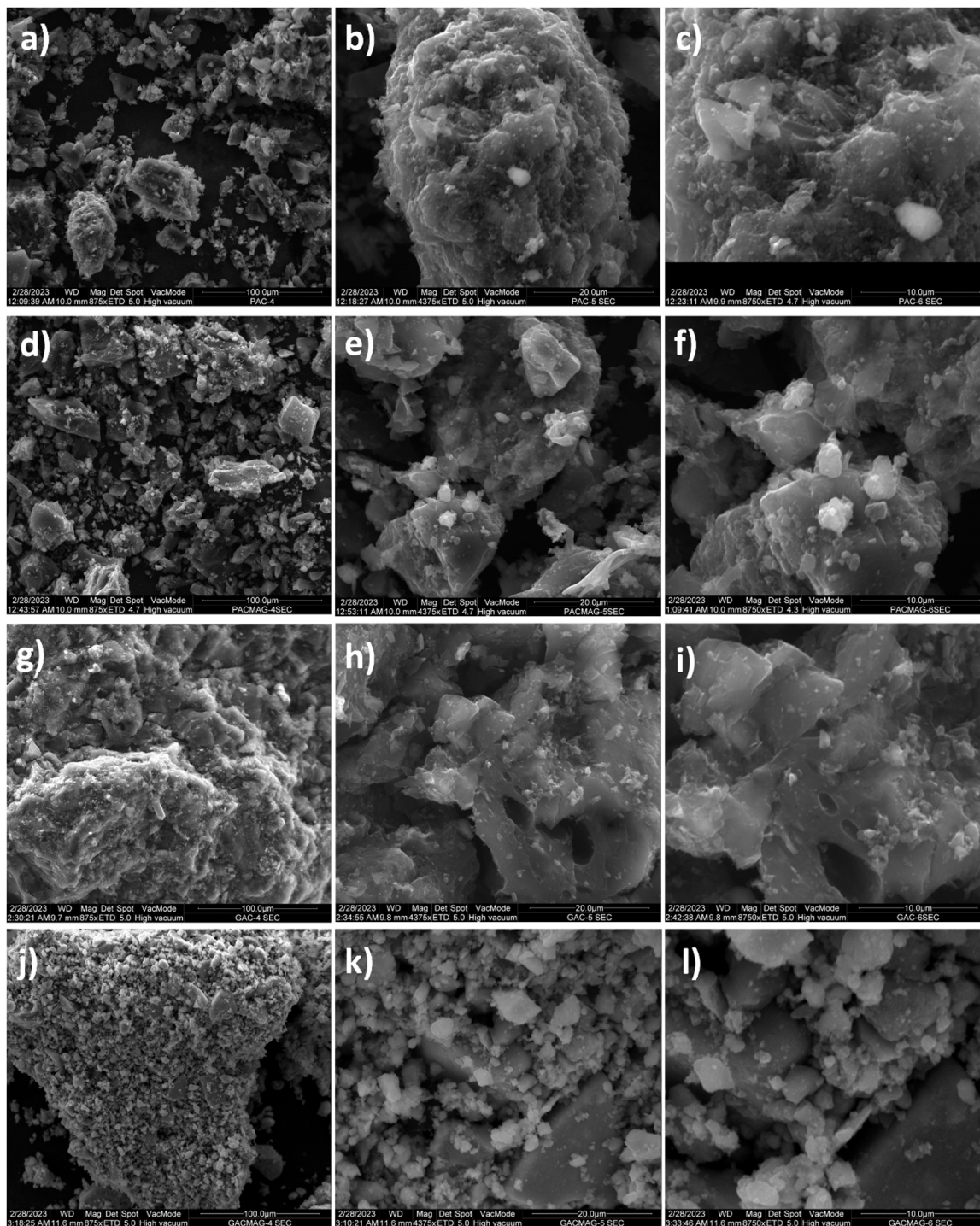
Fig. 1. SEM images of PAC (a, b, and c), PACMAG (d, e, and f), GAC (g, h, and i), and GACMAG (j, k, and l), at different magnifications (875X, 4375X, and 8750X), using the Everhart–Thornley detector.

3.2. Adsorption

3.2.1. Characterization of adsorbents

Fig. 1 shows the morphology of PAC, PACMAG, GAC, and GACMAG obtained by scanning electron microscope (SEM), at different magnifications. According to Fig. 1, PAC and PACMAG present irregular laminar structures. GAC and GACMAG have very rough surfaces and irregular cavities of different shapes. Compared to PAC and GAC, the SEM images of PACMAG (Fig. 1d, e, and f) and GACMAG (Fig. 1j, k, and l) show several clusters of bright particles of different dimensions. These clusters appear to be more evenly distributed over the activated carbon on GACMAG (Fig. 1j, k, and l) than on PACMAG (Fig. 1d, e, and f). It is expected that these clusters of bright particles are clusters of iron oxide NPs that have been incorporated into the surface of the activated carbon. It is not expected that these agglomerates of particles are activated carbon particles since they were still detected by the solid-state detector, which would not be possible if it was activated carbon (Fig. S2). Through FTIR analyses, Vargues et al. (2021) observed that iron oxide NPs were incorporated into PAC since an intense band near 600 cm^{-1} (indicative of Fe–O bond) was observed for PACMAG and iron oxide NPs, unlike PAC. For GAC/GACMAG/iron oxide NPs, the FTIR results (Fig. S3) confirm that these clusters of bright particles in GACMAG (Fig. 1j, k, and l) can be iron oxide nanoparticles since was also observed an intense band near 600 cm^{-1} (indicative of Fe –O bond) for GACMAG and iron oxide NPs, unlike GAC.

Table 2 gathers the A_{BET}, V_{total}, V_{meso}, V_{micro}, pH$_{PZC}$, moisture content, total ash content, and apparent density values, for the adsorbents used in this work. From the N$_2$ adsorption isotherm (Fig. S4) it is possible to verify that the incorporation of the magnetic NPs reflects in the decrease of the adsorption capacity, more pronounced for the GAC material. GAC presents a higher apparent surface area than PAC (Table 2). This is justified by the larger pore volume in GAC than in PAC (Table 2). In line with the analysis of the isotherms, the apparent surface area decreased from 650 to 548 m^2/g and from 906 to 655 m^2/g with the incorporation of iron oxide NPs in PAC and GAC, respectively. The same behavior was observed for the total pore volume. The values corroborate that in terms of percentage reduction in surface area or pore volume, these were greater for the incorporation of iron oxide NPs in GAC than for PAC. The reduction of the textural parameters after magnetization of the activated carbon materials results from a mass effect (the NPs are heavy particles and are less porous than the activated carbons) and possibly also some pore blocking (deposition of iron oxide NPs in the entrance of the activated carbon nanopores). However, the incorporation of iron oxide NPs in activated carbon contributed to the increase in the mesopores volumes (Table 2), which was also observed in literature studies [16,47]. The work by Labuto et al. [47] reports the mesoporous nature of the magnetic NPs and the consequent increase of the mesopore volume of the PAC after magnetization. Lompe et al. [16] observe the increase of the mesopore volume with an increase of the Fe$_2$O$_3$ mass fraction incorporated in PAC. For PACMAG or GACMAG, the volume of mesopores and micropores was similar while the PAC and GAC have a higher volume of micropores in line with their higher surface areas compared to the magnetic counterparts. The apparent surface areas and total pore volumes obtained for PACMAG or GACMAG in this work were slightly higher than the values that have been reported in the literature. For example, Shahrashoub and Bakhtiari [48] obtained an apparent surface area of 406 and 587 m^2/g, and total pore volumes of 0.34 and 0.29 cm^3/g for magnetite/PAC and GAC composites, respectively. Regarding the pH$_{PZC}$ of the adsorbents, it was observed that these values were slightly acidic for the granular materials (i.e., pH 6.8 for GAC and pH 6.3 for GACMAG) and slightly basic for the powdered counterparts (i.e., pH 8.1 for PAC and pH 7.3 for PACMAG). Since the pH values of the effluent to be treated are above the mentioned pH$_{PZC}$ values the surface will be negatively charged and thus more prone to the adsorption of cationic compounds. On the other hand, for effluent pH values below pH$_{PZC}$ the adsorbent surface will be positively charged favoring the adsorption of anionic compounds. In both activated carbons, the incorporation of iron oxide NPs nanoparticles in activated carbon also contributed to a slight decrease in pH$_{PZC}$ effect not always observed in the literature [47]. Regarding the particle size distribution for the adsorbents used, higher percentages of weight were observed in the range of 53–74 μm for PAC (Fig. S5) (corresponding to 42.4%) and in the range of 20–36 μm for PACMAG (Fig. S5) (corresponding to 34.0%). For GAC and GACMAG (Fig. S6) the highest weight percentage occurred for particle sizes > 850 μm (corresponding to 91.9% and 74.5% for GAC and GACMAG, respectively). The incorporation of iron oxide NPs in activated carbon contributed to the increase in the weight percentage of particles with smaller particle sizes (Figs. S5 and S6).

3.2.2. Effect of adsorbent concentration on COD removal and adsorption isothermal models

The influence of PAC, PACMAG, GAC, and GACMAG dosages on COD removal was studied (Fig. 2a and b). COD removals increased with the increase in the applied adsorbent dose, with COD removals varying between 38.6% and 59.7% for PAC (Figs. 2a), 39.3% and 61.9% for PACMAG (Figs. 2a), 59.0% and 83.0% for GAC (Fig. 2b), and 57.5% and 80.1% for GACMAG (Fig. 2b), in the dosage range of adsorbents studied. GAC and GACMAG were more efficient than PAC and PACMAG in removing COD. For PAC and PACMAG above the dosage of 70 g L^{-1} added, there was no significant change in the removal of COD. These results show that there is some organic matter that cannot be adsorbed by PAC and PACMAG. These differences in COD adsorption efficiency between PAC and GAC or between PACMAG and GACMAG may be due to the nature of the adsorbent (e.g., surface area, porosity, and pore size) and to the polarity and charge of the organic compounds [49]. In fact, GAC/GACMAG showed higher apparent surface area and total pore volume than PAC/PACMAG (Table 2). High values of apparent surface area and the presence of mesopores pores indicate a good potential for the removal of pollutants by adsorption [50]. As can be observed in Fig. 2a, the COD removal with or without incorporation of iron oxide NPs in PAC was similar. However, for GACMAG (Fig. 2b) a slight decrease (not significant, p < 0.05) in COD removal was observed when compared to GAC most probably because there was a greater reduction in the apparent surface area and volume of pores with the incorporation of iron oxide NPs in the GAC than in the PAC (Table 2). Considering the COD requirements for discharge (COD < 125 mg L^{-1}) and/or the

Table 2

Textural parameters, pH at the point of zero charge, moisture, and ash content for the listed activated carbon materials.

	A_{BET} (m^2/g)	V_{total}^a (cm^3/g)	V_{meso}^b (cm^3/g)	V_{micro}^c (cm^3/g)	pH$_{PZC}$	Moisture (%)	Ash (%)	Apparent density (kg/m^3)
PAC	650	0.39	0.14	0.25	8.1	7.3	13.2	560
PACMAG	548	0.36	0.18	0.18	7.3	6.0	35.0	639
GAC	906	0.50	0.18	0.32	6.8	12.7	8.0	491
GACMAG	655	0.43	0.22	0.21	6.3	6.9	31.1	580

Note:

[a] V_{total} evaluated at $p/p^0 = 0.975$ in the N$_2$ adsorption isotherms at − 196 °C

[b] V_{meso} – mesopore volume (2 < width < 50 nm), given by $V_{total} − V_{micro}$

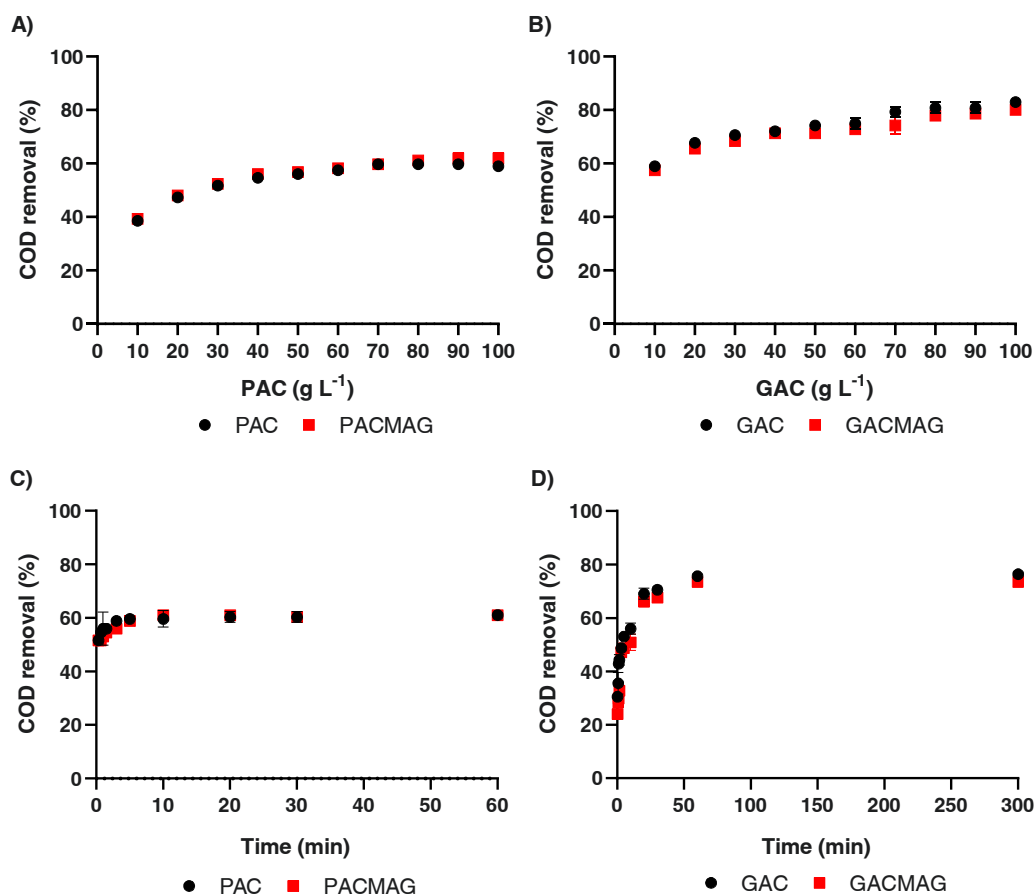[c] V_{micro} – total micropore volume (width < 2 nm)

Fig. 2. Effect of adsorbent dosage (10–100 g L^{-1}, using: a) PAC and PACMAG, and b) GAC and GACMAG, at mixing time = 13 h), and contact time (0–60 min, using: c) PAC and PACMAG at 70 g L^{-1}, and d) GAC and GACMAG at 60 g L^{-1}) on the COD removal (stirring speed = 250 rpm, temperature = 17.6 $\pm$ 0.1 ºC, COD = 458 $\pm$ 5 mg O$_2$ L^{-1}, pH = 7.91 $\pm$ 0.02).

maximum COD adsorption using the minimum adsorbent dosage, the doses 70 g L^{-1} for PACMAG and 60 g L^{-1} for GACMAG were chosen for the next experiments. In this way, PAC and GAC were used under the same doses of PACMAG and GACMAG, for comparison purposes. Using these doses, COD removals were 59.7 $\pm$ 1.0%, 59.7 $\pm$ 1.0%, 75.0 $\pm$ 2.1%, and 72.8 $\pm$ 1.0%, respectively, for PAC, PACMAG, GAC, and GACMAG. Thus, considering that the pairs of adsorbents (i.e., PAC-/PACMAG and GAC/GACMAG) were applied at the same dosage, these results show that the COD adsorption capacity by PACMAG or GACMAC was not influenced by the 23% substitution of activated carbon weight (PAC or GAC) by iron oxide NPs, despite the reduction in apparent surface area and total pore volume with the incorporation of NPs (Table 2). Therefore, this seems to point out that there was a synergistic effect between activated carbon (PAC or GAC) and the incorporated iron oxide NPs. Incidentally, an isolated experiment (results not yet disclosed) resulted in a COD removal of 41.2% of pretreated SWW by IOSLM+AC process (COD = 458 $\pm$ 5 mg O$_2$ L^{-1}), applying a dose of 60 g L^{-1} of iron oxide NPs and contact time of 1 h. Jain et al. [51] refer to iron oxide NPs as great adsorbents. The synergistic effect between activated carbon (PAC or GAC) and iron oxide NPs has been observed by some authors but there are also reports stating lower performance for the magnetic activated carbons. Affam [15] evaluated the COD removal from SWW by the adsorption process, using GAC and iron oxide-coated GAC at 3.5 g L^{-1}. The author observed that greater COD removals were obtained for iron oxide-coated GAC (ca. 70.7%) than for GAC (ca. 27.6%). Regarding PACMAG, Vargues et al. (2021) observed that the adsorption capacity of ibuprofen by PACMAG was not compromised with the incorporation of iron oxide NPs into PAC. However, for amoxicillin, these authors observed a slight decrease in the performance

of PACMAG in relation to PAC, indicating that the iron oxide NPs were distributed in macro and mesopores of the adsorbent, making it difficult for the large molecules (such as amoxicillin) to access some available active adsorption sites. Labuto et al. [47] also verified a decrease in the adsorption capacity of a PACMAG compared with the parent PAC being more pronounced for ibuprofen (negatively charged specie) than for caffeine a neutral specie. Authors propose the lower adsorption capacity of PACMAG to ibuprofen is due to the dominant mass effect of the NPs while for caffeine, smaller than ibuprofen, the more efficient packing in the micropore structure allows to overcome the mass effect. Kim et al. [52] also observed that PACMAG provided a lower removal of natural organic matter compared to PAC, derived from the reduction of micropore volume and surface area. On the other hand, Lompe et al. [16] state that a decrease in the removal of adsorbates with the incorporation of iron oxide NPs in PAC is not expected if small fractions of iron oxide NPs are used during the synthesis of iron oxide/activated carbon nanoparticle composite, or if PAC is highly mesoporous.

A set of isothermal models (Table S3) was studied to find the model that best fits the experimental data. Fig. 3a and b show the amount of COD adsorbed by PAC and PACMAG, and GAC and GACMAG, respectively, as a function of the final COD concentration. Using the Giles classification of adsorption isotherms from solute solutions [53], the adsorption isotherms shown in Fig. 3a and b are of types L1 and S1, respectively. The curvature presented by the type L1 shows that as more sites in the substrate are filled, it becomes increasingly difficult for a solute molecule to find an available vacant site [53]. On the other hand, the form S1 of isotherm indicates that the initial adsorption is low and increases as the number of adsorbed species increases. This means that there was an association between the adsorbed species, called
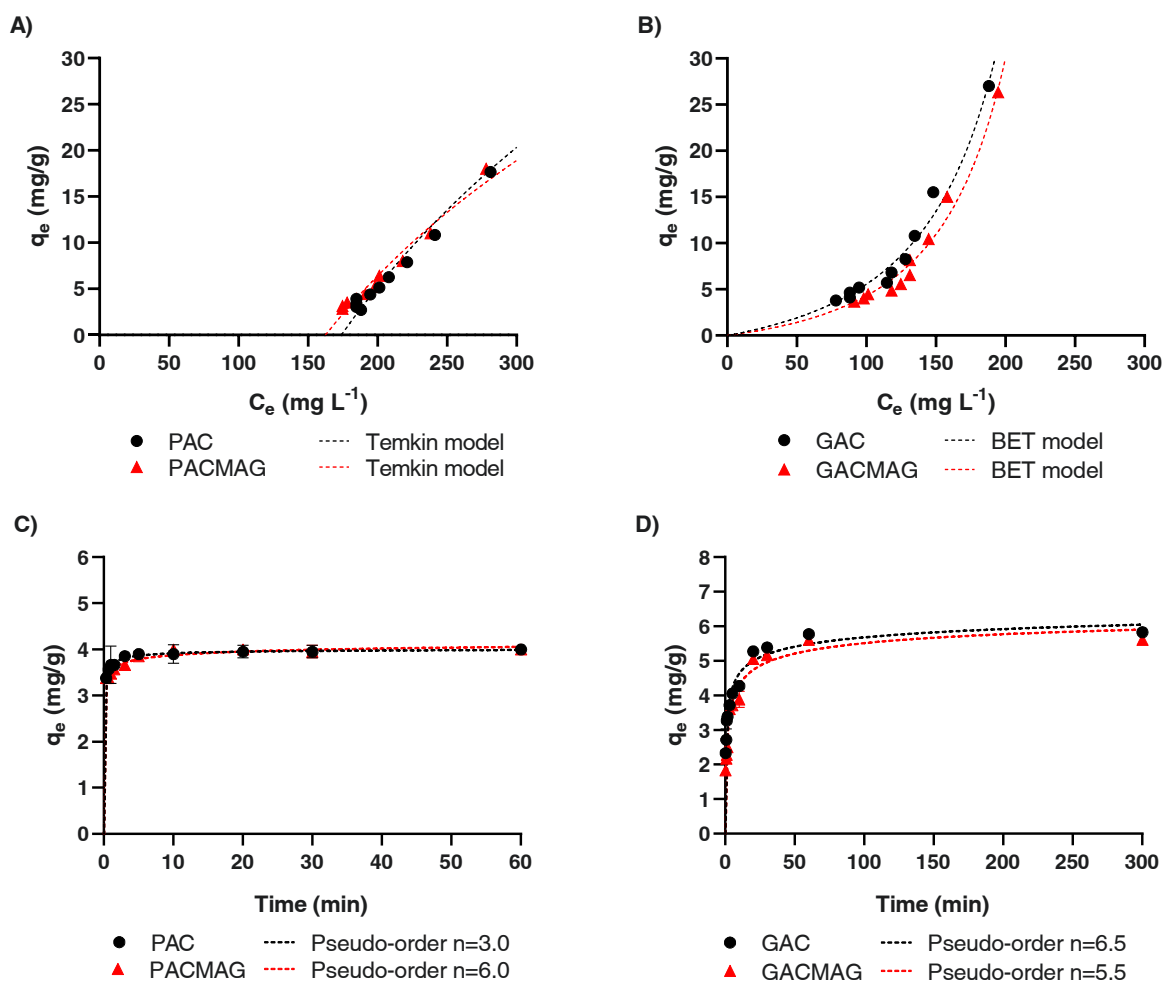
Fig. 3. Adsorption capacity (q_e) as a function of equilibrium concentration (C_e) (using: a) PAC and PACMAG, and b) GAC and GACMAG, at 10–100 g L^{-1} and mixing time = 13 h), and time (min) (using: c) PAC and PACMAG at 70 g L^{-1}, and d) GAC and GACMAG at 60 g L^{-1}) for the adsorption of COD (stirring speed = 250 rpm, temperature = 17.6 ± 0.1 ℃, COD = 458 ± 5 mg O_2 L^{-1}, pH = 7.91 ± 0.02).

cooperative adsorption, i.e., the adsorbed adsorbate affected the adsorption of other adsorbate molecules [54]. Considering the isotherm models studied (Table S5), it was observed that the model that would best fit the experimental data adequately were the Temkin model for PAC and PACMAG, and the BET model for GAC and GACMAG, achieving high correlation coefficients (R^2 of 0.9568, 0.9668, 0.9771, and 0.9769 for PAC, PACMAG, GAC, and GACMAG, respectively). A different result was observed by Vargues et al. [55]. These authors obtained different isothermal models between PAC and PACMAG, either in the adsorption of ibuprofen or amoxicillin, indicating that the structural changes introduced by magnetite seem to have an impact on the adsorption mechanism. This was not observed in this work, perhaps because the effluent used is very complex. The Temkin isotherm model, which presumes a multilayer adsorption process, postulates the following: i) as surface coverage increases, the heat of adsorption of all molecules in the layer decreases linearly rather than logarithmically, ii) the adsorption process is characterized by a uniform distribution of binding energies at the adsorbent surface, and iii) considers interactions between the adsorbent and the adsorbate [56,57]. The BET isotherm is based on the assumption that adsorption is multilayer [58]. GAC and GACMAG had a higher affinity with the organic matter than the PAC and PACMAG. This can be seen in Fig. 3a and b, where the experimental adsorption capacity of COD for the GAC (q_e = 27.0 mg g^{-1}) and GACMAG (q_e = 26.3 mg g^{-1}) were greater than that for the PAC (q_e = 5.1 mg g^{-1}) and PACMAG (q_e = 5.2 mg g^{-1}) at 200 mg L^{-1} of equilibrium concentration. The COD adsorption capacity values for GAC (q_e =70.97 mg g^{-1}) and

iron oxide-coated GAC (q_e = 181.67 mg g^{-1}) obtained by Affam [15] were much higher than the values obtained in this work, since the initial COD concentration, the adsorbent dosage and the effluent volume were different. Other factors such as pH, temperature, type of adsorbents, type of adsorbates, presence of several pollutants, contact time, surface functional group, and other experimental conditions can affect the adsorption process [19]. Low R^2 values were obtained for other models (*e.g.*, Langmuir isotherm, Redlich-Peterson, and others) (Table S5), which may be justified by the complexity of the effluent to be analyzed. By the way, Vargues et al. [55] obtained high coefficients of determination in several isothermal models also used in this work, probably due to the solutions prepared with only one contaminant, thus minimizing interference between adsorbates and between these and the adsorbent.

3.2.3. Effect of adsorption time on COD removal and the kinetics adsorption models

The effect of adsorption time on COD removal was studied (Fig. 2c and d). The maximum COD removal efficiency occurred at 5 min of contact time for PAC (ca. 59.7 ± 1.0%) and PACMAG (ca. 59.0 ± 0.0%), and at 60 min for GAC (ca. 75.7 ± 1.0%) and GACMAG (ca. 73.5 ± 2.1%). After this time, the system reaches equilibrium and the removal remains practically constant. In the first few minutes, the rapid increase in COD removal is due to the large empty adsorption sites and the high concentration gradient between the solution and the adsorbent. As the contact time increases, this gradient and the amount of available adsorption sites decrease, making the adsorption rates slower until the

process reaches equilibrium and the removal rate remains constant [59]. The adsorption kinetics of PAC and PACMAG were much faster than those of GAC and GACMAG since PAC and PACMAG present larger external areas and thus the active adsorption centers are more accessible to organic matter than GAC and GACMAG.

Adsorption kinetics is important in a wastewater treatment plant as it controls the efficiency of the process. Therefore, kinetic analysis was performed for PAC, PACMAG, GAC, and GACMAG using the kinetic adsorption models shown in Table S4, and the parameters calculated from the studied models are presented in Table S6. A very strong correlation coefficient ($0.8 \leq R^2 \leq 1.00$) was observed for the pseudo-second order (for PAC with R^2 of 0.9317, GAC with R^2 of 0.8498, and GACMAG with R^2 of 0.9030), Pseudo-order n (n ‡ 1) (for PAC with R^2 of 0.9810, PACMAG with R^2 of 0.9283, GAC with R^2 of 0.9673, and GACMAG with R^2 of 0.9600), Elovich (for PAC with R^2 of 0.8701, PACMAG with R^2 of 0.9039, GAC with R^2 of 0.9468, and GACMAG with R^2 of 0.9319), and Bangham models (for PAC with R^2 of 0.8575, PACMAG with R^2 of 0.8938, GAC with R^2 of 0.8929, and GACMAG with R^2 of 0.8578) (Table S6). According to Revellame et al. [60], $R^2 \geq 0.8$ indicates a good fit between the data and the model, but it is not enough to validate the choice of model, so it must be combined with other parameters. For example, it is usual to compare the adsorption capacity of the adsorbate obtained experimentally with the calculated value, to justify the fit of a model. Thus, according to the results in Table S6, the pseudo-order n kinetic model best fits the experimental data, for the PAC, PACMAG, GAC, and GACMAG. This model showed higher values of correlation coefficients close to 1 ($R^2 = 0.9810$ for PAC, $R^2 = 0.9283$ for PACMAG, $R^2 = 0.9673$ for GAC, and $R^2 = 0.9600$ for GACMAG) than the other models (see Fig. 3c and d). On the other hand, this kinetic model

also showed a calculated ($q_{cal.} = 4.04$ mg g^{-1} for PAC, $q_{cal.} = 4.47$ mg g^{-1} for PACMAG, $q_{cal.} = 7.71$ mg g^{-1} for GAC, and $q_{cal.} = 7.30$ mg g^{-1} for GACMAG) and experimental ($q_e = 3.90 \pm 0.07$ mg g^{-1} for PAC, $q_e = 3.86 \pm 0.00$ mg g^{-1} for the PACMAG, $q_e = 5.78 \pm 0.08$ mg g^{-1} for the GAG, and $q_e = 5.61 \pm 0.16$ mg g^{-1} for the GACMAG) adsorption capacity quite close. Vargues et al. [55] also observed that the adsorption of ibuprofen using PAC or PACMAG followed the pseudo-order n kinetic model. The pseudo-order n kinetic model predicts that the adsorption process is dependent on the adsorption capacity (i.e., that the rate-limiting step is chemisorption) and not on the adsorbate concentration [10]. Furthermore, this mechanism of adsorption occurs in two phases, the first being related to the diffusion of the pollutants from the solution to the adsorbent, and the second phase the fixation of the pollutants to the active sites available on the surface of the adsorbent [13]. According to Largitte & Pasquier [61], the pseudo-order n kinetic model assumes that: i) sorption only occurs on localized sites and involves no interaction between the sorbed ions; ii) the energy of adsorption is not dependent on surface coverage; iii) maximum adsorption corresponds to a saturated monolayer of adsorbates on the adsorbent surface; iv) the concentration of adsorbate is considered to be constant; and v) the adsorbate uptake on the activated carbons is governed by a rate equation of order n. In all kinetics models, lower AARD and E were found for PAC and PACMAG relative to GAC and GACMAG (Table S6).

3.2.4. Evaluation of different adsorbent separation methods

COD and turbidity removal by different adsorbent separation methods, namely: settling and magnetic separation over time (Fig. 4), and filtration (Table 3), using PAC, PACMAG, GAC, and GACMAG, were
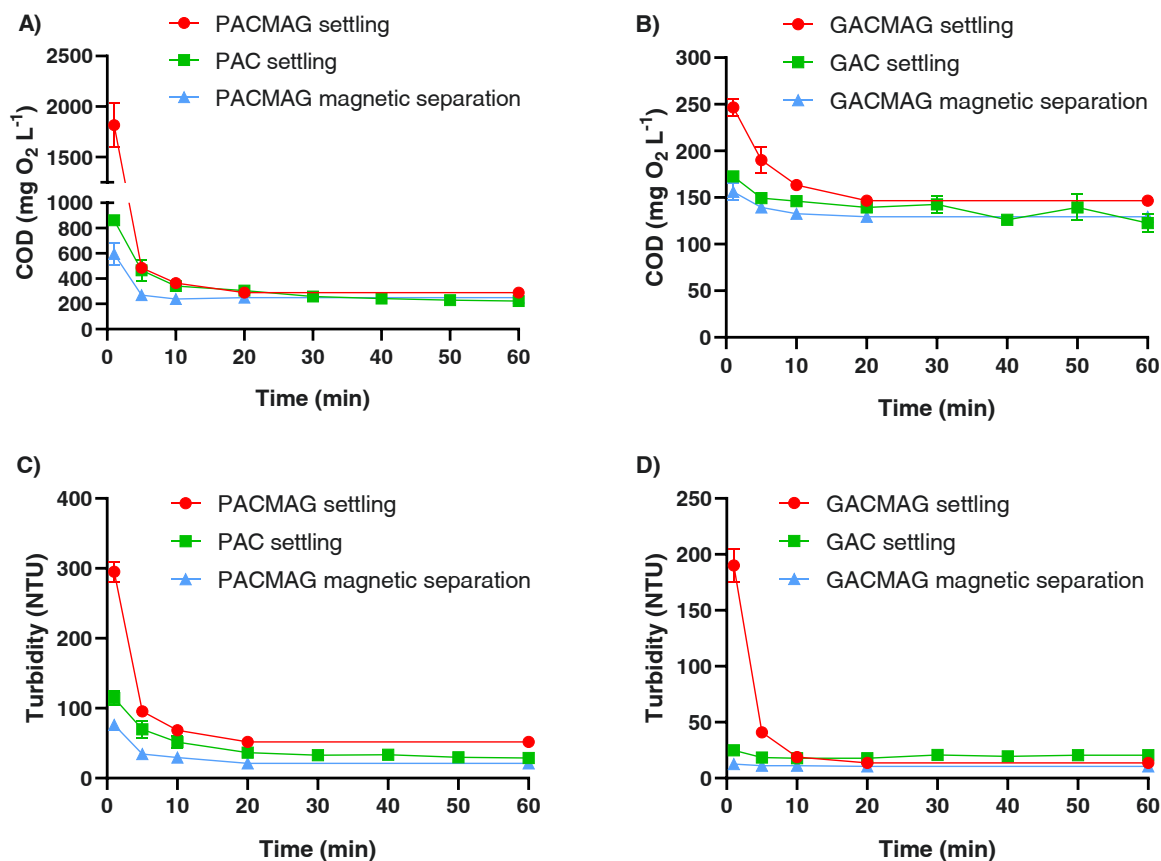

Fig. 4. Variation of the: a) COD concentration and c) turbidity using PACMAG and PAC; and b) COD concentration and d) turbidity using GACMAG and GAC with the magnetic separation and settling time. Adsorption operating conditions: stirring speed = 250 rpm, temperature = 18.9 ± 1.1 °C, mixing time = 5 min (for PAC and PACMAG) and 60 min (for GAC and GACMAG), adsorbent dosage = 70 g L^{-1} (for PAC and PACMAG) and 60 g L^{-1} (for GAC and GACMAG), COD = 467 ± 9 mg O$_2$ L^{-1}, and pH = 7.82 ± 0.01.

Table 3

COD, turbidity, and pH values obtained by adsorption-filtration process with PAC, PACMAG, GAC, and GACMAG, under operating conditions: stirring speed = 250 rpm, temperature = 18.9 ± 1.1 ºC, mixing time = 5 min (for PAC and PACMAG) and 60 min (for GAC and GACMAG), adsorbent dosage = 70 g L^{-1} (for PAC and PACMAG) and 60 g L^{-1} (for GAC and GACMAG), COD = 467 ± 9 mg O$_2$ L^{-1}, NH$_4^+$ = 8.9 ± 0.7 mg N L^{-1}, and pH = 7.82 ± 0.01.

Type of adsorbent	COD (mg O$_2$ L^{-1})	Turbidity (NTU)	NH$_4^+$ (mg N L^{-1})	pH
PAC	235 ± 7.1	0.253 ± 0.023	5.5 ± 0.8	9.42 ± 0.04
PACMAG	232 ± 9.4	0.272 ± 0.017	6.5 ± 0.4	8.23 ± 0.12
GAC	128 ± 2.4	0.227 ± 0.018	5.0 ± 0.8	8.82 ± 0.06
GACMAG	123 ± 9.4	0.291 ± 0.021	6.5 ± 0.4	7.90 ± 0.16

evaluated and compared. According to Fig. 4a, high COD concentrations (well above the COD concentration of the pretreated SWW, 467 ± 9 mg O$_2$ L^{-1}) were observed in the first minutes (between 0 and 5 min) of sedimentation (for PACMAG and PAC) or magnetic separation (for PACMAG), which indicates that the adsorbents used (PACMAG or PAC) were not yet completely separated from the effluent. For GACMAG or GAC, this did not occur as a faster separation of the adsorbent was observed (Fig. 4b). A decrease and stabilization of COD concentrations and turbidity over time were observed for all separation methods and adsorbents used. The magnetic separation method for PACMAG or GACMAG showed lower COD and turbidity values in the first minutes (0–20 min) than the settling separation method for PAC, PACMAG, GAC, or GACMAG. The minimum COD values reached in the magnetic separation method were 238 ± 0 mg O$_2$ L^{-1} (for PACMAG at 10 min) and 129 ± 0 mg O$_2$ L^{-1} (for GACMAG at 20 min). In the settling separation method, the following minimum COD values were 222 ± 9 mg O$_2$ L^{-1} (for PAC at 60 min), 288 ± 5 mg O$_2$ L^{-1} (for PACMAG at 20 min), 126 ± 5 mg O$_2$ L^{-1} (for GAC at 40 min), and 147 ± 0 mg O$_2$ L^{-1} (for GAC-MAG at 20 min). For PACMAG, no significant difference ($p < 0.05$) was observed between the filtration (COD = 232 ± 9 mg O$_2$ L^{-1}, Table 3) and the magnetic (COD = 238 ± 0 mg O$_2$ L^{-1} at 10 min, Fig. 4a) separation methods. Regarding GACMAG, no significant difference ($p < 0.05$) was observed between the filtration (COD = 123 ± 9 mg O$_2$ L^{-1}, Table 3) and the magnetic (COD = 129 ± 0 mg O$_2$ L^{-1} at 20 min, Fig. 4b) separation methods. The results also show that the settling separation method provides higher COD values than the filtration or magnetic separation methods when PACMAG and GACMAG are applied. This means that the effluent resulting from the settling separation method may have some easily non-settleable organic impurities, which affected the final COD concentration of the effluent. However, for PAC and GAC, there were no significant differences ($p < 0.05$) between the filtration (COD = 235 ± 7 mg O$_2$ L^{-1} and 128 ± 2 mg O$_2$ L^{-1} for PAC and GAC, respectively, Table 3) and settling separation method (COD = 222 ± 9 mg O$_2$ L^{-1} for PAC (at 60 min, Fig. 4a) and 126 ± 5 mg O$_2$ L^{-1} for GAC (at 40 min, Fig. 4b)). In fact, PACMAG and GACMAG had a higher weight percentage of smaller particles than PAC and GAC (Figs. S5 and S6), so a longer settling time for the former will be expected. Krahnstöver and Wintgens [62] state that PAC settling velocities are around 1 m/h for a particle size of 45 μm or 0.5 m/h for a particle size of 30 μm and even lower for the fine particle fraction. Generally, the sedimentation operation is subsequently associated with other PAC separation processes, such as deep bed filtration, lamella separator, pile cloth filtration, hydrocyclone, flotation, and microsieve [60], to prevent activated carbon of leaving the wastewater treatment plant.

According to Table 3, an increase in effluent pH after adsorption was observed for all adsorbents used. The increase in effluent pH may indicate that there was a loss of protons from the solution to the adsorbent, making the adsorbent surfaces more positively charged [63]. The observed ammonium nitrogen removal (Table 3) could be a reason for this increase in effluent pH. All studied adsorbents generate an effluent that meets the discharge pH requirements (pH<9.5).

3.3. Phytoremediation

3.3.1. Effect of bed depth and COD mass load on COD and ammonium nitrogen removal

The effect of bed depth on COD and ammonium nitrogen removal was analyzed for pretreated SWW by IOSLM + AC integrated process (trials A1 and B1 for CW1, and trials A2 and B2 for CW2) and for raw SWW (trials C1 for CW1 and C2 for CW2), at constant hydraulic loads (about 80 L m^{-2} d^{-1}) (Fig. 5). According to Fig. 5, it is observed that, for pretreated SWW, there are no significant differences ($p < 0.05$) in the COD removal efficiencies between tests A1 (83.8–88.3%) and A2 (89.9–95.0%). The same result was observed for ammonium nitrogen removal efficiencies between tests A1 (71.2–91.7%) and A2 (68.6–92.3%) as well as between tests B1 (44.8–68. 6%) and B2 (58.3–67.6%), which indicates that shallow beds may be sufficient to support low ammonium nitrogen mass loads. However, between tests B1 (59.8–78.6%) and B2 (81.5–90.8%) there were significant differences ($p < 0.05$) for COD removal efficiencies, indicating that the depth of the bed tested influenced the COD removal. For raw SWW, significant differences ($p < 0.05$) were observed in COD and ammonium nitrogen removal efficiencies between CW1 and CW2 (Fig. 5). In fact, no COD and ammonium nitrogen removal efficiencies were observed for CW1, but for CW2 these values ranged from 59.1% to 83.2% for COD and 51.9–64.5% for ammonium nitrogen (Fig. 5). Deeper beds allow a greater distribution of roots and microorganisms in the substrate, as well as greater HRT that allows a longer contact time between the microbiological community and the effluent to be treated, favoring a more complete degradation and/or assimilation of pollutants. HRT of about 3.6 ± 0.5 and 7.1 ± 0.9 h were determined for CW1 and CW2, respectively. Almeida et al. (2020) also observed greater nitrogen removals in deeper beds planted with *Vetiveria zizanioides*, in the treatment of synthetic effluent (68 ± 3–290 ± 8 mg NH$_4^+$-N L^{-1}). These authors concluded that deeper root systems are more favorable to the creation of zones with different oxidation conditions that lead to nitrogen removal. Mburu et al. [64]evaluated the effect of bed depth (from 0.65 to 0.8 m) and retention time (from 1 to 5 days) on the removal of COD, BOD$_5$, NH$_4^+$, and TSS from SWW, using vertical subsurface flow constructed wetland mesocosms without plants. These authors observed that, contrary to NH$_4^+$ and TSS removal, the effect of depth was insignificant in the removal of COD and BOD$_5$. However, an increase in retention time has a significant influence on the removal efficiency of organic matter, reaching removals of 50%, 55%, and 82% for BOD$_5$, COD, and TSS, respectively, on the 5th day of retention time.

According to Fig. 5, significant differences ($p < 0.05$) in the concentrations of COD and ammonium nitrogen were observed between the inlet and outlet effluents of the beds, for all tests (except for test C1). High COD (from 61% to 75%) and total nitrogen (from 47% to 62%) removals of poorly biodegradable SWW (BOD/COD ratio from 0.21 to 0.27) were also achieved by Odong et al. [21] when the authors tested constructed wetland planted with *M. violaceum*, *C. papyrus*, *P. mauritianus*, and *T. domingensis*. For biodegradable pretreated SWW from a biodigester, Manh et al. (2014) obtained COD and BOD removals around 60%, using CW planted with *Vetiveria zizanioides*.

The effect of COD loading on COD and ammonium nitrogen removal for pretreated SWW was evaluated, for both beds studied (Fig. 5). For CW1, an increase in COD load mass from 4.1 ± 0.5–9.5 ± 2.2 g m^{-2} d^{-1} had a significant effect ($p < 0.05$) on COD (Fig. 5a) and ammonium nitrogen (Fig. 5b) removal efficiency. Higher COD and ammonium nitrogen removal efficiencies were obtained when smaller COD loads applied were applied. For CW2, increasing COD mass load contributed to a significant ($p < 0.05$) decrease in the ammonium nitrogen removal efficiency but had no significant effect ($p < 0.05$) on COD removal efficiency. Therefore, it appears that ammonium nitrogen removal occurred in the presence of organic matter and with low dissolved oxygen. When the COD mass load of the beds was increased to 211.8 ± 26.4 g m^{-2} d^{-1}, a significant reduction in the removal efficiencies of
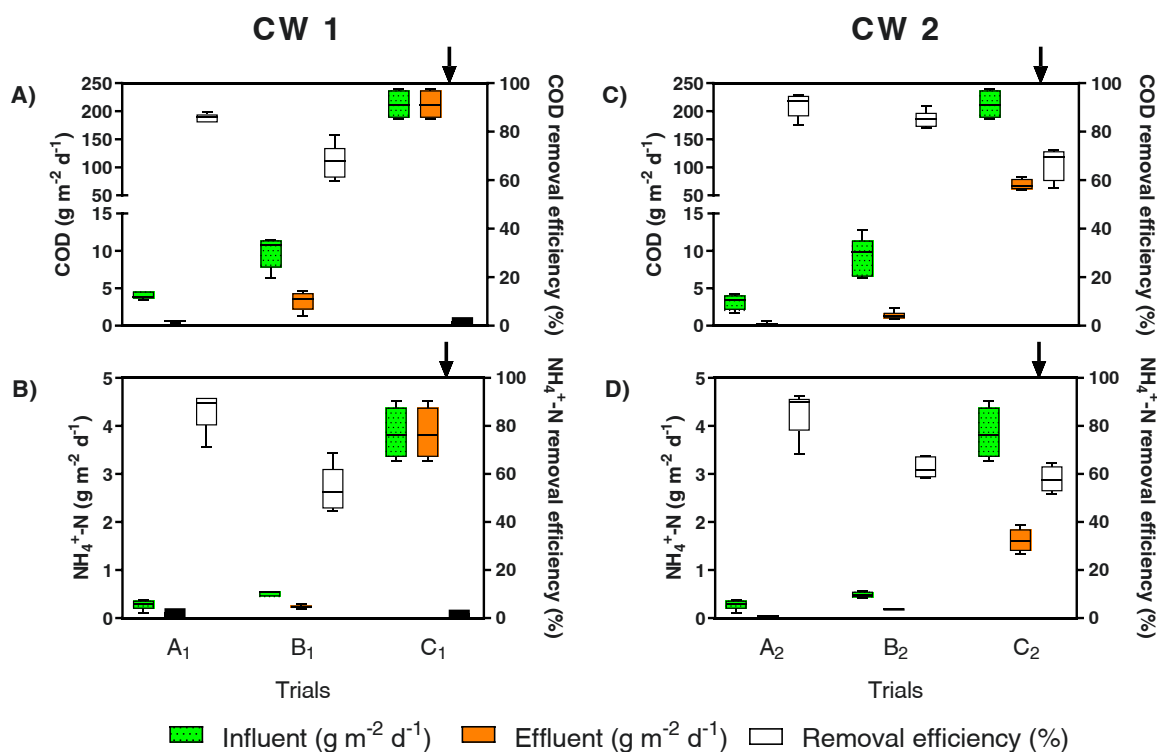
Fig. 5. Organic and ammonium load values in the inlet and outlet of CW 1 (A and B, respectively) and CW 2 (C and D, respectively), and the respective COD and ammonium removal efficiencies in different trials (A, B, and C). The average air and substrate temperature in the phytoremediation trials were 19.7 ± 3.9 and 15.9 ± 2.7 ºC, respectively.

COD and ammonium nitrogen was observed for both beds (except for ammonium nitrogen in the CW2) (Fig. 5d). Mburu et al. [64] report that a wide variation in the physicochemical characteristics of the SWW at the CW input can influence pollutant removal efficiencies.

The results show that only trials A1 (91 ± 11 mg O_2 L^{-1} for COD), A2 (41 ± 15 mg O_2 L^{-1} for COD), and B2 (86 ± 14 mg O_2 L^{-1} for COD) would be able to meet discharge requirements in terms of COD concentrations (COD ≤ 125 mg L^{-1}). On the other hand, the remaining tests, such as B1 (181 ± 52 mg O_2 L^{-1} for COD), C1 (2504 ± 321 mg O_2 L^{-1} for COD), C2 (1111 ± 24 mg O_2 L^{-1} for COD) resulted in effluents even with high concentrations of COD. The COD values in tests C1 and C2 show how important is to have a pretreatment by the IOSLM+AC process before the phytoremediation process. The IOSLM+AC processes have emerged as a pretreatment solution for high removals of organic matter, ammonia, and other compounds present in the effluent [46,5, 29]. Ramalho et al. [30] also noted the need for pretreatment by IOSLM+AC processes in the removal of organic matter and nitrogen from landfill leachate before the phytoremediation process with wetlands constructed with *Vetiveria zizanioides*.

Organic matter and ammonium nitrogen removal in the beds is associated with the occurrence of certain removal mechanisms. There are several indicators (e.g., pH, DO, potential redox) that can indicate the type of removal mechanisms that occurred in the bed. The removal of ammonium nitrogen could be due to ammonia volatilization [65] since the pH of the pretreated SWW (from tests A1, B1, A2, and B2) was still above 9.2 (that is, pH from which 50% of the ammoniacal nitrogen is available to be volatilized [66]). It is also expected that nitrogen removal may be associated with the nitrification process since the pH of the effluent decreased in all tests (Fig. 6a and e). Nitrification is a biological process of converting NH_4^+ to NO_3^- in two sequential steps in the presence of oxygen and results in the release of protons. In the first step, the biological oxidation of NH_4^+ to NO_2^- occurs by the action of bacteria of the genus *Nitrosomonas*, while in the second step, the oxidation of NO_2^- to NO_3^- occurs by the action of bacteria of the genus *Nitrobacter* [67]. On

the other hand, the decrease in pH can also be due to carbonation reactions or microbial degradation of organic matter. The removal of ammonium nitrogen may also be associated with plant assimilation [22]. Degradation of organic matter from poorly biodegradable wastewater in CW planted with *Vetiveria zizanioides* may be due to the release of plant enzymes. Enzymes released by plant roots can transform complex organic matter into simpler forms [68]. No significant difference ($p < 0.05$) between the inlet and outlet was observed for redox potential (Fig. 6b and f), conductivity (Fig. 6c and g), and DO (Fig. 6d and h), for both beds. As expected, significant oxygen consumption ($p < 0.05$) was observed in trials C1 and C2, due to the high concentrations of COD applied, reaching zero DO values in both beds (Fig. 6d and h). Dissolved oxygen consumption should be due primarily to the aerobic degradation of organic matter and then to the nitrification process. According to Soroko (2007), beds fed in vertical flow are favorable for carrying out aerobic processes since they allow intensive aeration caused by diffusion and convection phenomena.

3.3.2. Composition of plant biomass

Table 4 shows the biomass composition of the leaves of *Vetiveria zizanioides*, before and after the phytoremediation tests, for both beds studied. According to Table 4, the bed with greater depth (CW2) contributed significantly ($p < 0.05$) to a greater accumulation of nutrients in the leaves (such as calcium, potassium, and total nitrogen) than the beds with less depth (CW1). The accumulation of nutrients in the leaves of the *Vetiveria zizanioides* plant in deeper beds can be explained by the better root distribution of the plants, which leads to greater alternation of aerobic, anoxic, and anaerobic conditions inside the bed, and consequently a better symbiosis between plants and microorganisms. On the other hand, the decrease in phosphorus and sodium concentrations in the leaves for both beds could possibly be due to the low concentrations of these compounds in the applied wastewater. For example, phosphorus is a compound that is easily removed (98–99%) by the IOSLM process at pH 12 resulting in trace concentrations of
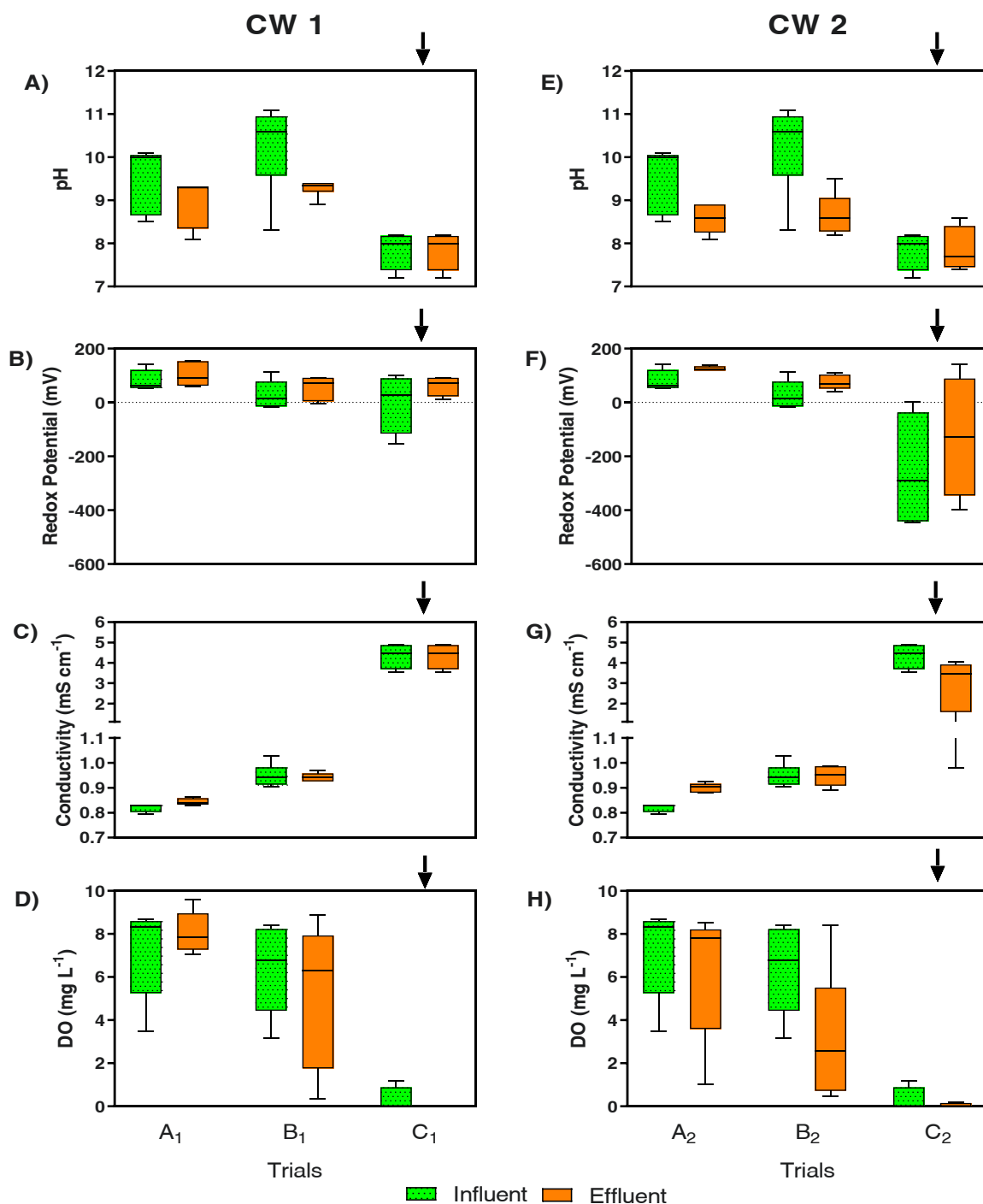
Fig. 6. pH, redox potential, conductivity, and DO values, in the inlet and outlet of CW 1 (A, B, C, and D, respectively) and CW 2 (E, F, G, and H, respectively), in different trials (A1, A2, B1, B2, C,1 and C2).

phosphorus [5]. Almeida et al. [31] also observed a decrease in the concentration of sodium and phosphorus in the leaves of *Vetiveria ziza-nioides*, when the authors applied synthetic wastewater in beds with different depths. During the phytoremediation tests, no signs of toxicity or chlorosis were detected in the leaves of *Vetiveria zizanioides*. The plants showed a very low growth rate (i.e., 0.4 ± 0.1 for CW1 and 0.5 ± 0.2 cm d^{-1} for CW2), maybe due to the season of the year (February to April), with average air and substrate temperatures in the phytor-emediation tests around 19.7 ± 3.9 and 15.9 ± 2.7 ºC, respectively. Even so, plant growth was not inhibited by the presence of high pH (around 10.25 ± 1.03), which could contribute to reduce the long time

of the carbonation process that has been observed in the literature. No significant differences ($p < 0.05$) in plant growth between beds were observed. However, Almeida et al. [31] concluded that the bed depth influenced plant growth, with values around 1.5 ± 0.1 cm d^{-1} for the deepest bed and 1.1 ± 0.1 cm d^{-1} for the shallower bed, in summer. The reason may be the bed depth that may limit the increase of the plant's root growth [69], which seems not to have occurred in this work.

4. Conclusion

The present work aimed to evaluate the effectiveness of the

Table 4 -

Leaves biomass composition for CW 1 and CW 2.

Parameter (mg g^{-1} DW)	Leaves biomass composition		
	Initial	Final	
		CW 1	CW 2
Ca^{2+}	1.20 ± 0.05	2.00 ± 0.09	2.30 ± 0.01
Mg^{2+}	0.04 ± 0.01	0.06 ± 0.01	0.07 ± 0.02
Na$^+$	0.45 ± 0.01	0.30 ± 0.01	0.36 ± 0.02
K$^+$	0.47 ± 0.02	3.14 ± 0.02	4.0 ± 0.02
TKN	10.50 ± 0.50	15.90 ± 0.20	17.60 ± 0.20
P	1.02 ± 0.01	0.20 ± 0.03	0.44 ± 0.03

Note: Mean ± Standard Deviation, calculated for a 95% confidence level; number of determinations (n = 3). DW – dried weight.

adsorption and the phytoremediation processes, as tuning processes in the removal of organic matter from a poorly biodegradable and alkaline pretreated SWW by an IOSLM and AC process. The following conclusions were drawn from this work:

- Under optimized conditions (dose and time), PAC and PACMAG were less effective than GAC and GACMAG in the removal of COD, being the COD adsorption capacity 3.90 ± 0.07 mg g^{-1} for PAC, 3.86 ± 0.00 mg g^{-1} for PACMAG, 5.78 ± 0.08 mg g^{-1} for GAG, and 5.61 ± 0.16 mg g^{-1} for GACMAG,
- COD adsorption capacity by PACMAG or GACMAC was not influenced by the impregnation of iron oxide NPs on PAC and GAC,
- Magnetic separation of PACMAG and GACMAG may replace the filtration separation method without changing the quality of the treated effluent,
- Bed depth and applied mass load are two factors that influence organic matter removal in constructed wetlands planted with *Vetiveria zizanioides*. Deeper beds and low COD loads contribute to greater efficiency of organic matter removal; thus, if the availability of land is a restriction, the option for deeper beds can be advantageous,
- *Vetiveria zizanioides* grew and showed no signs of toxicity when it was fed with very alkaline pretreated SWW (pH ≈ 10). The use of highly alkaline pretreated SWW could substantially reduce the time of the carbonation process,
- The adsorption process and the phytoremediation process can be tuned processes in the removal of organic matter from a poorly biodegradable and alkaline pretreated SWW from the IOSLM and AC integrated process and fulfill the discharge requirements in terms of COD (<125 mg L^{-1}).

The next works should focus on the evaluation of a) the adsorption of organic matter by GAC and GACMAG in adsorption columns, as well as its regeneration; b) the effect of temperature on the adsorption process; c) the effect of higher ratios PAC/iron oxide NPs and GAC/iron oxide NPs in the removal of organic matter; d) the COD removal with previous treatment with iron oxide NPs, before adsorption with PACMAG or GACMAG, to reduce the dosage of activated carbon; and e) the COD removal efficiency in CW planted with *Vetiveria zizanioides* in other seasons of the year.

CRediT authorship contribution statement

Luís Madeira: Conceptualization, Methodology, Investigation, Writing – original draft. **Adelaide Almeida**: Phytoremediation conceptualization, Writing – review & editing. **Ana Maria Rosa da Costa:** PACMAG and CAGMAG conceptualization, Adsorption isotherms and kinetics. **Ana S. Mestre:** PAC and GAC characterization analysis. **Fátima Carvalho**: Methodology, Writing – review & editing, Supervision, Funding acquisition. **Margarida Ribau Teixeira**: Conceptualization, Writing – review & editing, Funding acquisition, Supervision.

Declaration of Competing Interest

The authors declare that they have no known competing financial interests or personal relationships that could have appeared to influence the work reported in this paper.

Data availability

Data will be made available on request.

Appendix A. Supporting information

Supplementary data associated with this article can be found in the online version at doi:10.1016/j.jece.2023.110450.

References

[1] C.F. Bustillo-Lecompte, M. Mehrvar, Slaughterhouse wastewater characteristics, treatment, and management in the meat processing industry: A review on trends and advances, J. Environ. Manag. (2015), https://doi.org/10.1016/j. jenvman.2015.07.008.

[2] A.R. Prazeres, F. Fernandes, L. Madeira, S. Luz, A. Albuquerque, R. Simões, F. Beltrán, E. Jerónimo, J. Rivas, Treatment of slaughterhouse wastewater by acid precipitation (H2SO4, HCl and HNO3) and oxidation (Ca(ClO)₂, H2O2 and CaO₂), J. Environ. Manag. 250 (2019), 109558, https://doi.org/10.1016/j. jenvman.2019.109558.

[3] E. Bazrafshan, H.R. Zakeri, M.G.A. Vieira, Z. Derakhshan, L. Mohammadi, A. Mohammadpour, A. Mousavi Khaneghah, Slaughterhouse Wastewater Treatment by Integrated Chemical Coagulation and Electro-Fenton Processes, Page 11407 14, Sustain 2022 Vol. 14 (2022) 11407, https://doi.org/10.3390/ SU141811407.

[4] C.F. Bustillo-Lecompte, M. Mehrvar, E. Quiñones-Bolaños, Cost-effectiveness analysis of TOC removal from slaughterhouse wastewater using combined anaerobic-aerobic and UV/H2O2 processes, J. Environ. Manag. 134 (2014) 145–152, https://doi.org/10.1016/j.jenvman.2013.12.035.

[5] L. Madeira, F. Carvalho, A. Almeida, M. Ribau Teixeira, Optimization of atmospheric carbonation in the integrated treatment immediate one-step lime precipitation and atmospheric carbonation. The case study of slaughterhouse effluents, Results Eng. 17 (2023), 100807, https://doi.org/10.1016/J. RINENG.2022.100807.

[6] S. Al-Marri, S.S. Alquzweeni, K.S. Hashim, A. Matei, G. Racoviteanu, Review of the technologies for nitrates removal from water intended for human consumption, IOP Conf. Ser. Earth Environ. Sci. 664 (2021), 012024, https://doi.org/10.1088/ 1755-1315/664/1/012024.

[7] J.E. Foster, S. Mujovic, S. Krishnan, H. Rawindran, C.M. Sinnathambi, J.W. Lim, C. Mohan Sinnathambi, Comparison of various advanced oxidation processes used in remediation of industrial wastewater laden with recalcitrant pollutants, IOP Conf. Ser. Mater. Sci. Eng. 206 (2017), 012089, https://doi.org/10.1088/1757-899X/206/1/012089.

[8] A.R. Bracamontes-Ruelas, L.A. Ordaz-Díaz, A.M. Bailón-Salas, J.C. Ríos-Saucedo, Y. Reyes-Vidal, L. Reynoso-Cuevas, Emerging Pollutants in Wastewater, Advanced Oxidation Processes as an Alternative Treatment and Perspectives, Processes (2022), https://doi.org/10.3390/pr10051041.

[9] K. Keerthana, R. Thivyatharsan, Evaluation of the efficiency of constructed wetland and activated charcoal for the treatment of slaughterhouse wastewater, Earth, Energy Environ. 6 (2018) 12.

[10] T.R. Sahoo, B. Prelot, Adsorption processes for the removal of contaminants from wastewater: The perspective role of nanomaterials and nanotechnology. Nanomaterials for the Detection and Removal of Wastewater Pollutants, Elsevier,, 2020, pp. 161–222, https://doi.org/10.1016/B978-0-12-818489-9.00007-4.

[11] B.S. Rathi, P.S. Kumar, Application of adsorption process for effective removal of emerging contaminants from water and wastewater, Environ. Pollut. 280 (2021), 116995, https://doi.org/10.1016/J.ENVPOL.2021.116995.

[12] S.E. Agarry, C.N. Owabor, Evaluation of the Adsorption Potential of Rubber (*Hevea brasiliensis*) Seed Pericarp-Activated Carbon in Abattoir Wastewater Treatment and

in the Removal of Iron (III) Ions from Aqueous Solution, Niger. J. Technol. 31 (2012) 346–358, https://doi.org/10.4314/njt.v31i3.

[13] W.G. Djonga, E. Noubissié, G.B. Noumi, Removal of nitrogen, phosphate and carbon loads from slaughterhouse effluent by adsorption on an adsorbent based on Ayous sawdust (Triplochyton scleroxylon), Case Stud. Chem. Environ. Eng. (2021), https://doi.org/10.1016/j.cscee.2021.100120.

[14] J. del Real-Olvera, E. Rustrian-Portilla, E. Houbron, F.J. Landa-Huerta, Adsorption of organic pollutants from slaughterhouse wastewater using powder of Moringa oleifera seeds as a natural coagulant, Desalin. Water Treat. 57 (2016) 9971–9981, https://doi.org/10.1080/19443994.2015.1033479.

[15] A.C. Affam, Modification of granular activated carbon by aluminum and iron oxides for decontamination of poultry slaughterhouse wastewater using central composite design, Desalin. Water Treat. 177 (2020) 48–59, https://doi.org/10.5004/DWT.2020.25030.

[16] K.M. Lompe, D. Menard, B. Barbeau, The influence of iron oxide nanoparticles upon the adsorption of organic matter on magnetic powdered activated carbon, Water Res 123 (2017) 30–39, https://doi.org/10.1016/J.WATRES.2017.06.045.

[17] H.S. Park, J.R. Koduru, K.H. Choo, B. Lee, Activated carbons impregnated with iron oxide nanoparticles for enhanced removal of bisphenol A and natural organic matter, J. Hazard. Mater. 286 (2015) 315–324, https://doi.org/10.1016/J.JHAZMAT.2014.11.012.

[18] T.A. Aragaw, F.M. Bogale, B.A. Aragaw, Iron-based nanoparticles in wastewater treatment: A review on synthesis methods, applications, and removal mechanisms, J. Saudi Chem. Soc. 25 (2021), 101280, https://doi.org/10.1016/J.JSCS.2021.101280.

[19] M.E. Ali, M.E. Hoque, S.K. Safdar Hossain, M.C. Biswas, Nanoadsorbents for wastewater treatment: next generation biotechnological solution. Int. J. Environ. Sci. Technol. 17 (2020) 4095–4132, https://doi.org/10.1007/S13762-020-02755-4/TABLES/5.

[20] M. Soroko, Treatment of wastewater from small slaughterhouse in hybrid constructed wetlands systems. Ecohydrology and Hydrobiology, Polish Academy of Sciences,, 2007, pp. 339–343, https://doi.org/10.1016/S1642-3593(07)70117-9.

[21] R. Odong, F. Kansiime, J. Omara, J. Kyambadde, The potential of four tropical wetland plants for the treatment of abattoir effluent, Int. J. Environ. Technol. Manag. 16 (2013) 203–222, https://doi.org/10.1504/IJETM.2013.053640.

[22] R. Carreau, S. VanAcker, A.C. VanderZaag, A. Madani, A. Drizo, R. Jamieson, R.J. Gordon, Evaluation of a Surface Flow Constructed Wetland Treating Abattoir Wastewater, Appl. Eng. Agric. 28 (2012) 757–766, https://doi.org/10.13031/2013.42416.

[23] L.H. Manh, N.N.X. Dung, L. Van Am, B.T. Le Minh, Treatment of wastewater from slaughterhouse by biodigester and Vetiveria zizanioides L. L, Livest. Res. Rural Dev. 26 (2014).

[24] S.A. Ramos-Arcos, E. G. González-Mondragón, E. S. López-Hernández, A. R. Rodríguez-Luna, C. M. Morales-Bautista, S. Lagunas-Rivera, S. López-Martínez, Phytoremediation Potential of Chrysopogon zizanioides for Toxic Elements in Contaminated Matrices. Biodegradation Technology of Organic and Inorganic Pollutants, IntechOpen,, 2022, https://doi.org/10.5772/intechopen.98235.

[25] L.T. Danh, P. Truong, R. Mammucari, T. Tran, N. Foster, Vetiver grass, Vetiveria zizanioides: A choice plant for phytoremediation of heavy metals and organic wastes, Int. J. Phytoremediat. 11 (2009) 664–691, https://doi.org/10.1080/15226510902787302.

[26] E. Fasani, G. DalCorso, A. Zerminiani, A. Ferrarese, P. Campostrini, A. Furini, Phytoremediatory efficiency of Chrysopogon zizanioides in the treatment of landfill leachate: a case study, Environ. Sci. Pollut. Res. Int. 26 (2019) 10057–10069, https://doi.org/10.1007/S11356-019-04505-7.

[27] A.Y. Goren, A. Yucel, S.C. Sofuoglu, A. Sofuoglu, Phytoremediation of olive mill wastewater with Vetiveria zizanioides (L.) Nash and Cyperus alternifolius L. Environ, Technol. Innov. (2021) 24, https://doi.org/10.1016/j.eti.2021.102071.

[28] R. Seroja, H. Effendi, S. Hariyadi, Tofu wastewater treatment using vetiver grass (Vetiveria zizanioides) and zeliac, Appl. Water Sci. 8 (2018) 1–6, https://doi.org/10.1007/S13201-018-0640-Y/TABLES/3.

[29] L. Madeira, F. Carvalho, M.R. Teixeira, C. Ribeiro, A. Almeida, Vertical flow constructed wetland as a green solution for low biodegradable and high nitrogen wastewater: A case study of explosives industry, Chemosphere 272 (2021), 129871, https://doi.org/10.1016/j.chemosphere.2021.129871.

[30] M. Ramalho, T. Jovanović, A. Afonso, A. Baía, A. Lopes, A. Fernandes, A. Almeida, F. Carvalho, Landfill leachate treatment by immediate one-step lime precipitation, carbonation, and phytoremediation fine-tuning, Environ. Sci. Pollut. Res 1 (2022) 1–10, https://doi.org/10.1007/S11356-022-18729-7/TABLES/3.

[31] A. Almeida, K. Jóźwiakowski, A. Kowalczyk-Juśko, P. Bugajski, K. Kurek, F. Carvalho, A. Durao, C. Ribeiro, M. Gajewska, Nitrogen removal in vertical flow constructed wetlands: influence of bed depth and high nitrogen loadings, Environ. Technol. (U. Kingd.) 41 (2020) 2196–2209, https://doi.org/10.1080/09593330.2018.1557749.

[32] R. Baird, A.D. Eaton, E.W. Rice, L. Bridgewater, American Public Health Association, American Water Works Association, Water Environment Federation. Standard Methods for the Examination of Water and Wastewater, 23rd ed. ed..,, American Public Health Association, American Water Works Association, Water Environment Federation,, 2017.

[33] M.A. Tabatabai, Handbook of Reference Methods for Plant Analysis, Crop Sci. 38 (1998) 1710–1711, https://doi.org/10.2135/cropsci1998.0011183×003800060050x.

[34] ISO9277. Determination of Specific Surface Area of Solids by Gas Adsorption - BET Method, Second ed..,, ISO,, Switzerland, 2010.

[35] J. Rouquerol, P. Llewellyn, F. Rouquerol, Is the BET equation applicable to microporous adsorbents? in: P.L. Llewellyn, F. Rodriquez Reinoso, J. Rouqerol, N.

[36] S. (Eds.), Charact. Porous Solids Vii - Proc. 7th Int. Symp. . Charact. Porous Solids (2006) 49–56.

[36] M. Thommes, K. Kaneko, A.V. Neimark, J.P. Olivier, F. Rodriguez-Reinoso, J. Rouquerol, K.S.W. Sing, Physisorption of gases, with special reference to the evaluation of surface area and pore size distribution (IUPAC Technical Report), Pure Appl. Chem. 87 (2015) 1051–1069, https://doi.org/10.1515/PAC-2014-1117/MACHINEREADABLECITATION/RIS.

[37] J. Rouquerol, F. Rouquerol, P. Llewellyn, G. Maurin, K.S. Sing, Adsorption by powders and porous solids: principles, methodology and applications, Academic Press,, 2013.

[38] F. Rodriguez-Reinoso, J.M. Martin-Martinez, C. Prado-Burguete, B. McEnaney, A standard adsorption isotherm for the characterization of activated carbons, J. Phys. Chem. 91 (1987) 515–516, https://doi.org/10.1021/J100287A006/ASSET/J100287A006.FP.PNG_V03.

[39] J.S. Noh, J.A. Schwarz, Estimation of the point of zero charge of simple oxides by mass titration, J. Colloid Interface Sci. 130 (1989) 157–164, https://doi.org/10.1016/0021-9797(89)90086-6.

[40] A.S. Mestre, J. Pires, J.M.F. Nogueira, J.B. Parra, A.P. Carvalho, C.O. Ania, Waste-derived activated carbons for removal of ibuprofen from solution: Role of surface chemistry and pore structure, Bioresour. Technol. 100 (2009) 1720–1726, https://doi.org/10.1016/J.BIORTECH.2008.09.039.

[41] A.S. Mestre, R.M.C. Viegas, E. Mesquita, M.J. Rosa, A.P. Carvalho, Engineered pine nut shell derived activated carbons for improved removal of recalcitrant pharmaceuticals in urban wastewater treatment, J. Hazard. Mater. 437 (2022), 129319, https://doi.org/10.1016/J.JHAZMAT.2022.129319.

[42] AWWA, Standard for Powdered Activated Carbon, American Water Works Association,, Denver, Colorado, 1996.

[43] CEFIC, 1986, Test methods for activated carbon, Conseil Européen des Fédérations de l'Industrie Chimique (European Council of Chemical Manufacturers' Federation).

[44] R.M.C. Viegas, A.S. Mestre, E. Mesquita, M. Campinas, M.A. Andrade, A. P. Carvalho, M.J. Rosa, Assessing the applicability of a new carob waste-derived powdered activated carbon to control pharmaceutical compounds in wastewater treatment, Sci. Total Environ. 743 (2020), 140791, https://doi.org/10.1016/J.SCITOTENV.2020.140791.

[45] M. Ng, S. Dalhatou, J. Wilson, B.P. Kamdem, M.B. Temitope, H.K. Paumo, H. Djelal, A.A. Assadi, P. Nguyen-tri, A. Kane, Characterization of Slaughterhouse Wastewater and Development of Treatment Techniques: A Review, Processes (2022), https://doi.org/10.3390/pr10071300.

[46] L. Madeira, A. Almeida, M. Ribau Teixeira, A. Prazeres, H. Chaves, F. Carvalho, Immediate one-step lime precipitation and atmospheric carbonation as pre-treatment for low biodegradable and high nitrogen wastewaters: A case study of explosives industry, J. Environ. Chem. Eng. 8 (2020), 103808, https://doi.org/10.1016/j.jece.2020.103808.

[47] G. Labuto, A.P. Carvalho, A.S. Mestre, M.S. dos Santos, H.R. Modesto, T.D. Martins, S.G. Lemos, H.D.T. da Silva, E.N.V.M. Carrilho, W.A. Carvalho, Individual and competitive adsorption of ibuprofen and caffeine from primary sewage effluent by yeast-based activated carbon and magnetic carbon nanocomposite, Sustain. Chem. Pharm. 28 (2022), 100703, https://doi.org/10.1016/j.scp.2022.100703.

[48] M. Shahrashoub, S. Bakhtiari, The efficiency of activated carbon/magnetite nanoparticles composites in copper removal: Industrial waste recovery, green synthesis, characterization, and adsorption-desorption studies, Microporous Mesoporous Mater. 311 (2021), 110692, https://doi.org/10.1016/J.MICROMESO.2020.110692.

[49] P. Lawtae, C. Tangsathitkulchai, The use of high surface area mesoporous-activated carbon from longan seed biomass for increasing capacity and kinetics of methylene blue adsorption from aqueous solution, Molecules (2021) 26, https://doi.org/10.3390/molecules26216521.

[50] R. Vinayagam, S. Pai, G. Murugesan, T. Varadavenkatesan, S. Narayanasamy, R. Selvaraj, Magnetic activated charcoal/Fe2O3 nanocomposite for the adsorptive removal of 2,4-Dichlorophenoxyacetic acid (2,4-D) from aqueous solutions: Synthesis, characterization, optimization, kinetic and isotherm studies, Chemosphere (2022) 286, https://doi.org/10.1016/j.chemosphere.2021.131938.

[51] M. Jain, M. Yadav, T. Kohout, M. Lahtinen, V.K. Garg, M. Sillanpää, Development of iron oxide/activated carbon nanoparticle composite for the removal of Cr(VI), Cu(II) and Cd(II) ions from aqueous solution, Water Resour. Ind. 20 (2018) 54–74, https://doi.org/10.1016/J.WRI.2018.10.001.

[52] S. Kim, J. Kim, G. Seo, Iron oxide nanoparticle-impregnated powder-activated carbon (IPAC) for NOM removal in MF membrane water treatment system, N. pub Balaban 51 (2013) 6392–6400, https://doi.org/10.1080/19443994.2013.781000.

[53] C.H. Giles, T.H. MacEwan, S.N. Nakhwa, D. Smith, 786. Studies in adsorption. Part XI. A system of classification of solution adsorption isotherms, and its use in diagnosis of adsorption mechanisms and in measurement of specific surface areas of solids, J. Chem. Soc. (1960) 3973–3993, https://doi.org/10.1039/JR9600003973.

[54] S. Liu, Cooperative adsorption on solid surfaces, J. Colloid Interface Sci. 450 (2015) 224–238, https://doi.org/10.1016/J.JCIS.2015.03.013.

[55] F. Vargues, M.A. Brion, A.M. Rosa da Costa, J.A. Moreira, M. Ribau Teixeira, Development of a magnetic activated carbon adsorbent for the removal of common pharmaceuticals in wastewater treatment, Int. J. Environ. Sci. Technol. 18 (2021) 2805–2818, https://doi.org/10.1007/S13762-020-03029-9/FIGURES/9.

[56] M.T. Amin, A.A. Alazba, M. Shafiq, Adsorptive removal of reactive black 5 from wastewater using bentonite clay: Isotherms, kinetics and thermodynamics, Sustainability 7 (2015) 15302–15318, https://doi.org/10.3390/su71115302.

[57] S. Kalam, S.A. Abu-Khamsin, M.S. Kamal, S. Patil, Surfactant Adsorption Isotherms: A Review, ACS Omega 6 (2021) 32342, https://doi.org/10.1021/ACSOMEGA.1C04661.

[58] A. Ebadi, J.S. Soltan Mohammadzadeh, A. Khudiev, What is the correct form of BET isotherm for modeling liquid phase adsorption? Adsorption 15 (2009) 65–73, https://doi.org/10.1007/S10450-009-9151-3/METRICS.

[59] M.I. Konggidinata, B. Chao, Q. Lian, R. Subramaniam, M. Zappi, D.D. Gang, Equilibrium, kinetic and thermodynamic studies for adsorption of BTEX onto Ordered Mesoporous Carbon (OMC,). J. Hazard. Mater. 336 (2017) 249–259, https://doi.org/10.1016/J.JHAZMAT.2017.04.073.

[60] E.D. Revellame, D.L. Fortela, W. Sharp, R. Hernandez, M.E. Zappi, Adsorption kinetic modeling using pseudo-first order and pseudo-second order rate laws: A review, Clean. Eng. Technol. 1 (2020), 100032, https://doi.org/10.1016/J.CLET.2020.100032.

[61] L. Largitte, R. Pasquier, A review of the kinetics adsorption models and their application to the adsorption of lead by an activated carbon, Chem. Eng. Res. Des. 109 (2016) 495–504, https://doi.org/10.1016/j.cherd.2016.02.006.

[62] T. Krahnstöver, T. Wintgens, Separating powdered activated carbon (PAC) from wastewater – Technical process options and assessment of removal efficiency, J. Environ. Chem. Eng. 6 (2018) 5744–5762, https://doi.org/10.1016/J.JECE.2018.09.001.

[63] L.S. Čerović, S.K. Milonjić, M.B. Todorović, M.I. Trtanj, Y.S. Pogozhev, Y. Blagoveschenskii, E.A. Levashov, Point of zero charge of different carbides,

Colloids Surf. A Physicochem. Eng. Asp. 297 (2007) 1–6, https://doi.org/10.1016/J.COLSURFA.2006.10.012.

[64] C. Mburu, J. Kipkemboi, R. Kimwaga, Impact of substrate type, depth and retention time on organic matter removal in vertical subsurface flow constructed wetland mesocosms for treating slaughterhouse wastewater, Phys. Chem. Earth 114 (2019), 102792, https://doi.org/10.1016/j.pce.2019.07.005.

[65] A.C. VanderZaag, R.J. Gordon, D.L. Burton, R.C. Jamieson, G.W. Stratton, Ammonia Emissions from Surface Flow and Subsurface Flow Constructed Wetlands Treating Dairy Wastewater, J. Environ. Qual. 37 (2008) 2028–2036, https://doi.org/10.2134/JEQ2008.0021.

[66] L. Lin, S. Yuan, L. Lin, S. Yuan, J. Chen, Z. Xu, X. Lu, Removal of ammonia nitrogen in wastewater by microwave radiation, J. Hazard. Mater. 161 (2009) 1063–1068, https://doi.org/10.1016/j.jhazmat.2008.04.053.

[67] J. Vymazal, Removal of nutrients in various types of constructed wetlands, Sci. Total Environ. 380 (2007) 48–65, https://doi.org/10.1016/J.SCITOTENV.2006.09.014.

[68] A.K.E. Tjelldén, S.M. Kristiansen, H. Matthiesen, O. Pedersen, Impact of roots and rhizomes on wetland archaeology: A review, Conserv. Manag. Archaeol. Sites. (2015), https://doi.org/10.1080/13505033.2016.1175909.

[69] J. Vymazal, Constructed Wetland with Emergent Macrophytes: From Experiments to a High Quality Treatment Technology., 10th International Conference on Wetland Systems for Water Pollution Control,, Lisbon, Portugal, 2006, pp. 1611–1621.